Bypassing the Multi-reference Character of Singlet Molecular Oxygen. Part 2: Ene-reaction

Malte F. Jespersen, Emma Amalie Petersen-Sonn, Solvejg Jørgensen, Matthew S. Johnson, and Kurt V. Mikkelsen*

Department of Chemistry, University of Copenhagen, Universitetsparken 5, DK-2100 Copenhagen, Denmark

E-mail: kmi@chem.ku.dk

Abstract

Theoretical calculations involving singlet molecular oxygen ($O_2(^1\Delta_g)$) are challenging due to their inherent multi-reference character. We have tested the quality of restricted and unrestricted DFT geometries obtained for the reaction between singlet oxygen and a series of alkenes (propene, 2-methylpropene, *trans*-butene, 2-methylbutene and 2,3-dimethylbutene) which are able to follow the ene-reaction. The electronic energy of the obtained geometries are refined using 3 different methods which account for the multi-reference character of singlet oxygen. The results show that the mechanism for the ene-reaction is qualitatively different when either one or two allylic-hydrogen groups are available for the reaction. When one allylic-hydrogen group is available the UDFT calculations predict a stepwise addition forming a biradical intermediate, while, the RDFT calculations predict a concerted reaction where both hydrogen abstraction and oxygen addition occur simultaneously. When two allylic-hydrogen groups are available for the reaction then UDFT and RDFT predict the same reaction mechanism, namely that the reaction occurs as a stepwise addition without a stable intermediate between the two transition states. The calculated rate constants are in reasonable agreement with experimental data, except for *trans*-butene where the calculated rate constant is three orders of magnitude lower than the experimental one. In conclusion we find that the simple bypassing scheme tested in this paper is a robust approach for calculations of reaction involving singlet oxygen in the limit that the transition state processes low multi-reference character.

Introduction

Molecular oxygen has played a central role in the biological and geological evolution of the planet.[1] While low levels of molecular oxygen (O_2) are generated in a CO_2 atmosphere,[2] photosynthesis allowed considerable amounts to accumulate once oceanic iron was oxidised.[3] In terms of gas phase chemistry, Chapman[4] showed how the ozone layer formed which shields life from harmful UV radiation. Thus, life has evolved in the context of the photochemistry of O, O_2 and O_3 including their excited states.[5] Molecular oxygen has a unique chemistry due in large part to its triplet ground state. The triplet ground state ($^3\Sigma_g^-$) shows a low rate of reaction with most stable compounds in the environment even though the thermodynamic driving force is large. The lowest electronically excited state of molecular oxygen, (called herein 'singlet oxygen', $^1\Delta_g$) has a lifetime that is long enough to allow for bimolecular reactions and it is known to be reactive towards alkenes and sulfides.

The atmospheric concentration of singlet oxygen is 10^8 (molecules/cm^3)[6] which is larger than the concentration of the main atmospheric oxidant the OH radical with a concentration around 10^6 (molecules/cm^3).[7] However, speaking broadly, its lower reactivity means that a negligible amount of VOC will react with singlet oxygen in the free atmosphere.[8] This conclusion would not pertain in local environments with elevated singlet oxygen, or for compounds with a $^1O_2$ reaction rate ca 100 times faster than their OH reaction rate. Also recent experiments have indicated that reaction with singlet oxygen is important for some compounds in atmospheric aerosol.[9]

The reaction between singlet oxygen and ethene is generally thought to follow a (2+2) cyclo-addition mechanism forming dioxethane.[10] Dioxethane is thermally unstable and decomposes into two formaldehyde molecules. Alkenes containing an allylic hydrogen can follow the ene-mechanism in which singlet oxygen adds to the double bond and abstracts the allylic hydrogen. The product of the reaction is a hydroperoxide in which the double

bond has migrated by one carbon relative to the reagent.[10] The (2+2) cyclo-addition and ene-reaction mechanisms compete and are generally believed to proceed through different transition states. Dioxethane formation is found to be favoured in polar solvents indicating a larger degree of charge separation in the (2+2) cyclo-addition transition state.[11,12]

In this work we focus on the ene-reaction. We investigate a series of alkenes (propene, 2-methylpropene, *trans*-butene, 2-methylbutene and 2,3-dimethylbutene) created by adding methyl groups sequentially to ethene. The behaviour across this set of alkenes can be used as a proxy for the reactivity of similar alkenes.

There is debate regarding whether singlet oxygen addition to an alkene is concerted or stepwise. Early theoretical results indicated the formation of a diradical intermediate.[13–16] In contrast, experiments indicate either a perepoxide intermediate or a concerted reaction.[10,17–22] The measurement of the deuterium kinetic isotope effect for *cis*- and *trans*-deuterated 2,3-dimethylbutene provided an important breakthrough. No preference in the product distribution was observed for *cis*-2,3-dimethylbutene while for *trans*-2,3-dimethylbutene hydrogen abstraction was favoured over deuterium.[18] This observation was perceived as clear evidence for the peroxide intermediate mechanism.

First we will present the computational method, and then discuss the results across the series of reactions tested in this work. Finally, we will make general conclusions about the performance of the tested methods. Based on the theoretical results, predictions of the reaction mechanism for the addition reaction of singlet oxygen to allylic alkenes are made.

Computational Method

Gaussian 16[23] is used for all geometry calculations, employing the density functional theory (DFT) functionals ωB97XD,[24] M06-2X[25] and B3LYP[26] in connection with the aug-cc-pVTZ (AVTZ) basis set.[27] The empirical dispersion function D3 is added to the B3LYP functional to give the full B3LYP-D3 abbreviation. The effect of changing the grid spacing is tested by applying the superfine grid for the ωB97XD and M06-2X functionals. Both restricted (RDFT) and broken symmetry unrestricted (UDFT) calculations are performed on singlet oxygen and transition states. For the alkene it is assumed that the UDFT solution is identical to RDFT, based on its closed shell structure. Broken symmetry solutions of the UDFT wave functions suffer from spin contamination where higher spin states are mixed in the wave function. Systems containing singlet oxygen are often heavily spin contaminated and corrections need to be applied. Yamanaka et al. developed an approximate spin projection scheme to remove the spin contamination error from the UDFT wavefunction (AP-UDFT).[28] Later Saito et al. developed an approximate spin projection optimization scheme where the spin contamination error is removed from the gradient and Hessian.[29] Studies of the reaction of singlet oxygen with ethylene show that approximate spin projection optimization should be performed to obtain accurate geometries for the initial TS, which is the rate limiting step of the reaction. Unfortunately, the AP-UDFT optimization scheme is not readily available in any commercial electronic structure packages. The lack of availability often limits the use of AP-UDFT for geometry optimizations. Instead AP-UDFT is often used to correct only the electronic energy of spin contaminated UDFT geometries.[30–32] We have chosen to perform the optimization with RDFT and UDFT. The electronic energies of the obtained DFT geometries are refined with 3 different methods, which are described next.

Method 1: the multi-reference character of singlet oxygen is treated directly by refining the energy with the MRCI+Q/AVTZ or CASPT2/AVTZ method.[33,34] MRCI and CASPT2 use a CASSCF wave function as the reference wave function,[35] and require a selection of

an active space. To ensure a comparable selection of the active space across the different chemical systems an RHF calculation is performed on top of the optimized DFT geometries. Then, the RHF orbitals are localized following the localization procedure proposed by Pipek and Mezey.[36] The localized orbitals are manually inspected and an active space consisting of ten electrons in seven orbitals (10,7) is selected. The active space contains six electrons in the four π/π^* orbitals of singlet oxygen, from the alkene, three orbitals are selected, which contains the four electrons located in the π and the C-H σ orbital involved in the hydrogen abstraction and the empty π^* orbital. The localized orbitals are used as a starting guess for the state averaged CASSCF calculations which include the three lowest singlet states of molecular oxygen as well as the triplet state, and span all the low lying electronic states of molecular oxygen ($<$ 40 kcal/mol). The state averaged CASSCF wavefunction is used as the reference function for single state MRCI/AVTZ and CASPT2/AVTZ calculations of the triplet state and the three lowest singlet states of the system. The Davidson correction is used to improve the size extensivity of the MRCI calculation.[37] MRCI is not a size consistent method, and the reactants are calculated in a single calculation where the species are moved 30 Angstroms apart to minimize interactions between the reactant moieties.

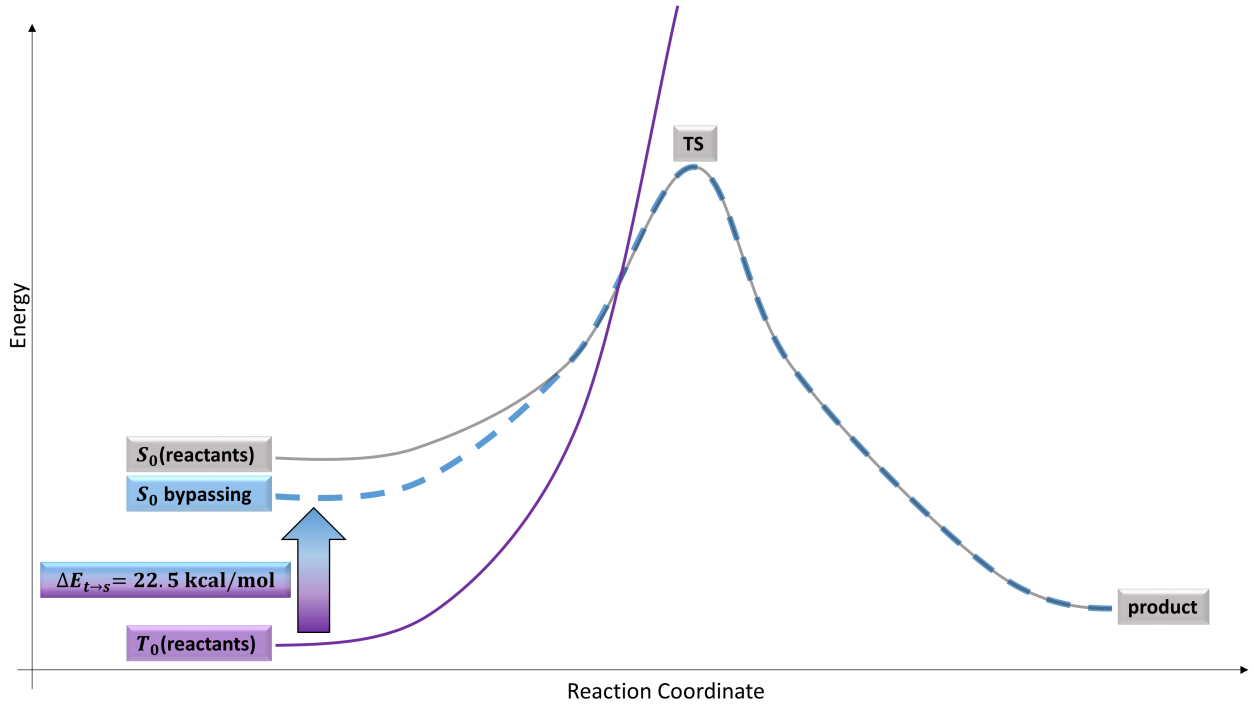

Figure 1: Illustration of the bypassing scheme, T_0 and S_0 are the potential energy surface of the triplet and singlet ground states, calculated with a restricted method. S_0 bypassing is the hypothetical potential energy surface where the error due to the multi-reference character of singlet molecular oxygen is removed. $\Delta E_{t\to s}$ is the experimentally determined singlet/triplet splitting of molecular oxygen.

Method 2: The multi reference character of singlet oxygen is bypassed by performing the electronic structure calculations using the triplet state rather than the singlet. Triplet oxygen is optimized with the RODFT method and the energy is refined using single point ROCCSD(T)-F12a/VDZ-F12 or ROCCSD(T)/AVTZ energies to which the experimentally determined singlet/triplet splitting of 22.5 kcal/mol is added, effectively obtaining the electronic energy of singlet oxygen. The bypassing scheme is shown in Figure 33.

Method 3: this method is intermediate between methods 1 and 2: the electronic energy is calculated as the sum of the triplet CCSD(T)/AVTZ energy, and the singlet/triplet energy splitting is calculated using either CASPT/AVTZ or MRCI+Q/AVTZ. Methods 2 and 3 exploit the fact that ground state triplet oxygen should be accurately described with a

single reference method. CCSD(T)/AVTZ should capture most of the dynamic correlation of the system, whereas the singlet/triplet energy splitting obtained from experiment or by MRCI/CASPT2 calculations deals with the multi-reference character of the system.

Method 2 is a straightforward approach for handling the multi-reference character of singlet oxygen, whereas methods 1 and 3 are much more delicate procedures where the selection of the active space is both time-consuming and biased by the required manual inspection of the localized orbitals. The complexity of methods 1 and 3 imply that they are only used to refine the electronic energies of the geometries optimized with the B3LYP-D3/AVTZ method.

CCSD(T)-F12a/VDZ-F12 energies are calculated for all optimized reactants and transition states. Single point CCSD(T)/AVTZ, MRCI/AVTZ and CASPT2/AVTZ calculations are performed for each point along the intrinsic reaction coordinate (IRC) calculated with B3LYP-D3/AVTZ. CCSD(T)-F12a/VDZ-F12, CCSD(T)/AVTZ, CASPT2/AVTZ and MRCI+Q/AVTZ calculations are performed using Molpro2012.[38] The multi-reference character of the transition state (TS) is addressed using the T_1 diagnostic, and from the spin contamination calculated from the expectation value of the $\left\langle \hat{S}^2 \right\rangle$ of the UDFT wavefunction.

Rate constants for the studied reactions are calculated using transition state theory:

$$k = L\kappa \frac{k_b T}{h} \frac{Q_{\mathrm{TS}}}{Q_{\mathrm{R}} Q_{^1\mathrm{O}_2}} \mathrm{e}^{-\frac{E_0}{k_B T}}$$

where k_B, T and h are Boltzmann's constant, the temperature and Planck's constant respectively. $\frac{Q_{\mathrm{TS}}}{Q_{\mathrm{R}} Q_{^1\mathrm{O}_2}}$ is the ratio of the partition functions for the TS and the two reactants, and E_0 is the electronic energy barrier including zero point vibrational energy (ZPVE). κ is the one dimensional Eckart tunnelling correction which is calculated from the imaginary frequency of the transition state and the height of the forward and reverse barriers. L is the

symmetry number of the reaction.

Result and Discussion

In the following section the results of the different test systems will be presented system by system starting with the smallest, propene + singlet oxygen, and ending with 2,3-dimethylbutene. Based on the results shown in the following section we present, in the final section, conclusions regarding the computational approaches.

Propene

Propene is the smallest system able to follow the ene-reaction mechanism. Various reaction mechanisms have been suggested for the reaction between propene and singlet oxygen. The propene + singlet oxygen reaction has been studied by Maranzana et al.[13] They applied two theoretical approaches, denoted here as method A and B.

Method A: optimizes the geometries with restricted and unrestricted DFT, applying the B3LYP and MPW1K functionals in connection with the 6-311G(d,p) basis set. The energies of the optimized geometries were corrected using approximate spin projection methods.

Method B: multi-reference calculations are performed where the geometries are optimized with (10,8)CASSCF and the energy is refined using (12,12)CASPT2. Maranzana et al.[13] find that the reaction proceeds through two transition states where the first transition state is the O_2 addition to the double bond forming a biradical intermediate, and the second transition state connects the biradical intermediate with the products through hydrogen abstraction. The first step of this reaction path has a barrier of (12-16) kcal/mol while the second step has a low barrier of (1-4) kcal/mol. Hence, the initial TS leading to formation of the biradical intermediate is the rate determining step for the reaction. The authors also find a concerted

reaction path with the RB3LYP/6-311G(d,p) method connecting propene and singlet oxygen directly to the hydroperoxide product. However, they argue that the transition state is an artefact of the applied RDFT methods, since the wavefunction is unstable towards orbital rotation, and the concerted TS could not be optimized at the CASSCF level of theory. The study by Maranzana et al. also included an investigation of several alternative reaction paths. One of these is a two step mechanism where the first step is abstraction of the allylic hydrogen forming HO_2 + the allylic radical, followed by radical recombination. The energy barrier for this reaction was calculated to be (23.9-33.6) kcal/mol and was deemed too high to be important for the overall reaction mechanism. The possible formation of a perepoxide intermediate was also investigated since experimental kinetic isotope effects could indicate formation of a perepoxide intermediate.[19,17] However, the calculations show that the perepoxide intermediate is 12 kcal/mol higher in energy compared to the biradical intermediate, and is not important for the reaction mechanism.[13]

Based on the work of Maranzana et al. the radical recombination pathway is excluded from this study. The remaining reaction paths, studied in this paper, can be divided into two classes: singlet oxygen approaching the alkene on the same side as the allylic group (*cis*), or approaching the alkene from the opposite side of the allylic group (*trans*). In the following the *cis*-TS and *trans*-TS structures are studied using methods 1, 2 and 3 and the results are compared to those of Maranzana et al. Since all the methods are different the important differences are analyzed and discussed. Methods 1, 2, 3 and A are based on DFT optimizations and method B is based on CASSCF optimization. Method 1 and B refine the electronic energies by including dynamic correlation in the multi-reference calculation by MRCI or CASPT2. Method A refines the energy using the approximate spin projection method. Methods 2 and 3 bypass the multi-reference character of singlet oxygen by adding the calculated or experimentally determined singlet/triplet splitting to triplet state molecular oxygen, and dynamic correlation is added with the CASPT2, MRCI+Q and/or CCSD(T)

methods.

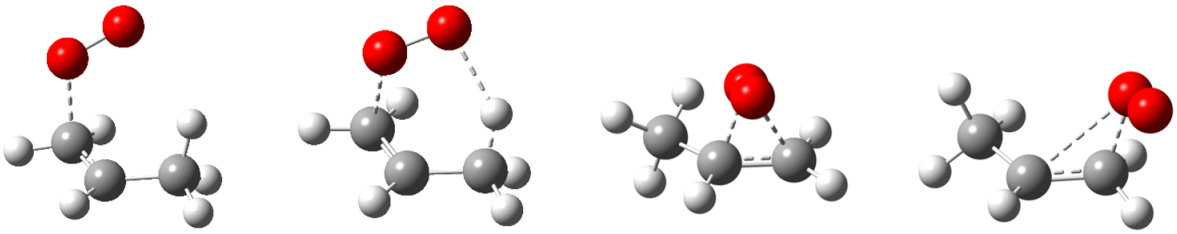

Figure 2: TS structure of *cis*-TS-UDFT (left), *cis*-TS-RDFT (left to the middle), *trans*-TS-RDFT (right to the middle) and *trans*-TS-UDFT (right), calculated at (R/U)B3LYP-D3/AVTZ level of theory.

Optimizations applying the three tested DFT functionals all show the same qualitative features:

cis-addition: RDFT finds one concerted TS which connects the reactants directly with hydroperoxide product (*cis*-TS-RDFT). The UDFT method is unable to locate the concerted TS but converge to a TS (*cis*-TS-UDFT) which connects the reactants with a biradiral/zwitter-ionic intermediate.

trans-addition: RDFT finds a transition state which forms the perepoxide. UDFT finds a transition state which leads to a biradiral/zwitter-ionic intermediate.

Figure 34 shows the optimized TS structures for the *cis* and *trans*-addition of singlet oxygen to propene obtained at RB3LYP-D3/AVTZ and UB3LYP/AVTZ which illustrates the differences of the optimized geometries with RDFT and UDFT methods.

Table 1: Calculated spin contamination($\langle S^2 \rangle$), T_1 diagnostics and energy barriers calculated with CCSD(T)-F12a/VDZ-F12//DFT/AVTZ using method 2 for energy refinement (E_0) and rate constants k for the *cis*-addition of singlet oxygen to propene.

Propene + $^1O_2$ (*cis*-TS)	$\langle S^2 \rangle$	T_1	E_0 (kcal/mol)	k ($\frac{cm^3}{s}$)
RM06-2X		0.025	13.35	2.99×10^{-24}
RM06-2X*		0.025	13.34	2.97×10^{-24}
RωB97XD		0.027	13.23	3.18×10^{-24}
RωB97XD*		0.027	13.22	3.26×10^{-24}
RB3LYP-D3		0.028	13.09	4.38×10^{-24}
UM06-2X	0.989	0.079	16.95	3.10×10^{-26}
UωB97XD	1.000	0.095	15.98	1.43×10^{-25}
UB3LYP-D3	0.934	0.076	14.49	1.65×10^{-24}

$*$: The geometry optimization was done using the superfine grid.

cis-Addition

Only the *cis*-approach mechanism is believed to follow the ene-reaction pathway, and this path will be the starting point for the following discussion. The spin contamination and T_1 diagnostics are used to estimate the quality of the single reference wave function. A singlet state should have $\left\langle \hat{S}^2 \right\rangle = 0$ and the deviation from this number is an indication for whether higher spin states are mixed with the wave function (spin contamination). The T_1 diagnostic is a measure of whether multi-reference character is affecting the CCSD(T) wave function. $T_1 < 0.02$ and $T_1 < 0.03$ are the generally accepted limits for closed shell species and open shell species respectively.[39,40] When the T_1 diagnostic exceeds the threshold value, then the multi-reference character of the system is likely to affects the quality of the CCSD(T) energies and multi-reference methods should be applied. We emphasize that the multi-reference character will likely disappear at the TS region since the origin of the multi-reference character is the degeneracy of the HOMO and LUMO orbitals in singlet molecular oxygen, a degeneracy which is lost as oxygen approaches the alkene to from the TS. Furthermore, the hydroperoxide formed in the ene-reaction (the ene-product) is a closed shell structure which should be accurately described by single reference methods. The reaction path goes from a multi-reference problem in the reactant region to a single-reference description in the prod-

uct region. The TS is located in between these two areas, and the success of the bypassing scheme used in method 2 depends on whether the multi-reference character persists in the TS or not. Table 1 shows the spin contamination, T_1 diagnostics, energy barriers and rate constants for the TS found for the *cis*-addition of singlet oxygen to propene. The result for *cis*-UDFT-TS will be presented next, followed by the results for *cis*-RDFT-TS:

cis-TS-UDFT

The *cis*-TS-UDFT calculations leading to a biradical/zwitterion intermediate have T_1 diagnostics in the range (0.076-0.095) which is much higher than the generally expected value for a single-reference system. Consequently, large uncertainties are expected for these calculations and multi-reference methods should to be applied to obtain reliable results. To further investigate the reaction coordinate, UB3LYP-D3/AVTZ is taken as a general representative for the energy surfaces obtained with the UDFT method. Using the intrinsic reaction coordinate (IRC) from this methods, the energy of the singlet surface is further refined by methods 1-3. All energy refinements along the reaction coordinate are calculated using the AVTZ basis set to eliminate any basis set effect. Method 1 is used to calculate the energy of the three lowest singlet states as well as the triplet energy. The relative energies of the exited states are important indicators for the extent of the multi-reference character for the system.

The surfaces of S_0, S_1, S_2 and T_0 are shown in Figure 35, where S_1 and S_2 refer to the first and second excited singlet states, and S_0 and T_0 are the lowest energy singlet and triplet states, respectively. The S_0, S_1, and T_0 surfaces remain close in energy, especially S_0 and T_0 which end up with an energy difference of 4.81 and 4.20 kcal/mol at the CASPT2/AVTZ and MRCI+Q/AVTZ levels of theory, respectively. The small energy separation between S_0 and T_0 for the biradical/zwitterionic product enables efficient quenching back to the triplet state. Reformation of the triplet state reactants from the triplet state biradical is associated with an energy barrier of 0.31 kcal/mol at the CASPT2/AVTZ theory, while this

path is fully repulsive at MRCI+Q/AVTZ. The H-shift-TS which connects the biradical with the ene-product is located 2.13 and 6.59 kcal/mol (CASPT2/AVTZ and MRCI+Q/AVTZ, method 1) lower in energy than the biradical, which indicates that the biradical is not a stable intermediate along the reaction coordinate.

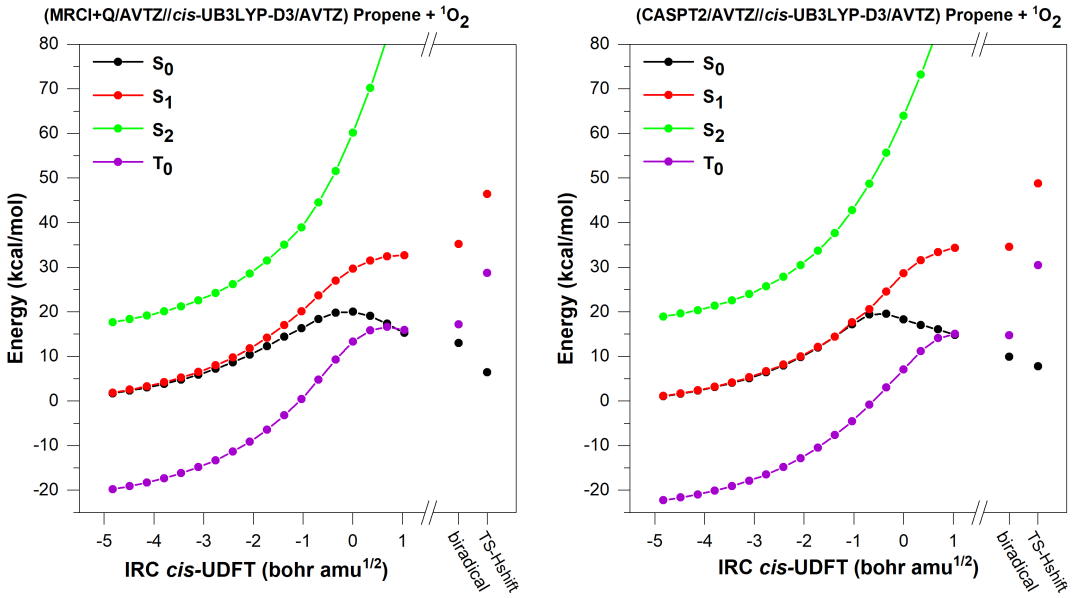

Figure 3: S_0, S_1, S_2 and T_0 electronic energy surfaces calculated by method 1 along the reaction coordinate of *cis*-UDFT.

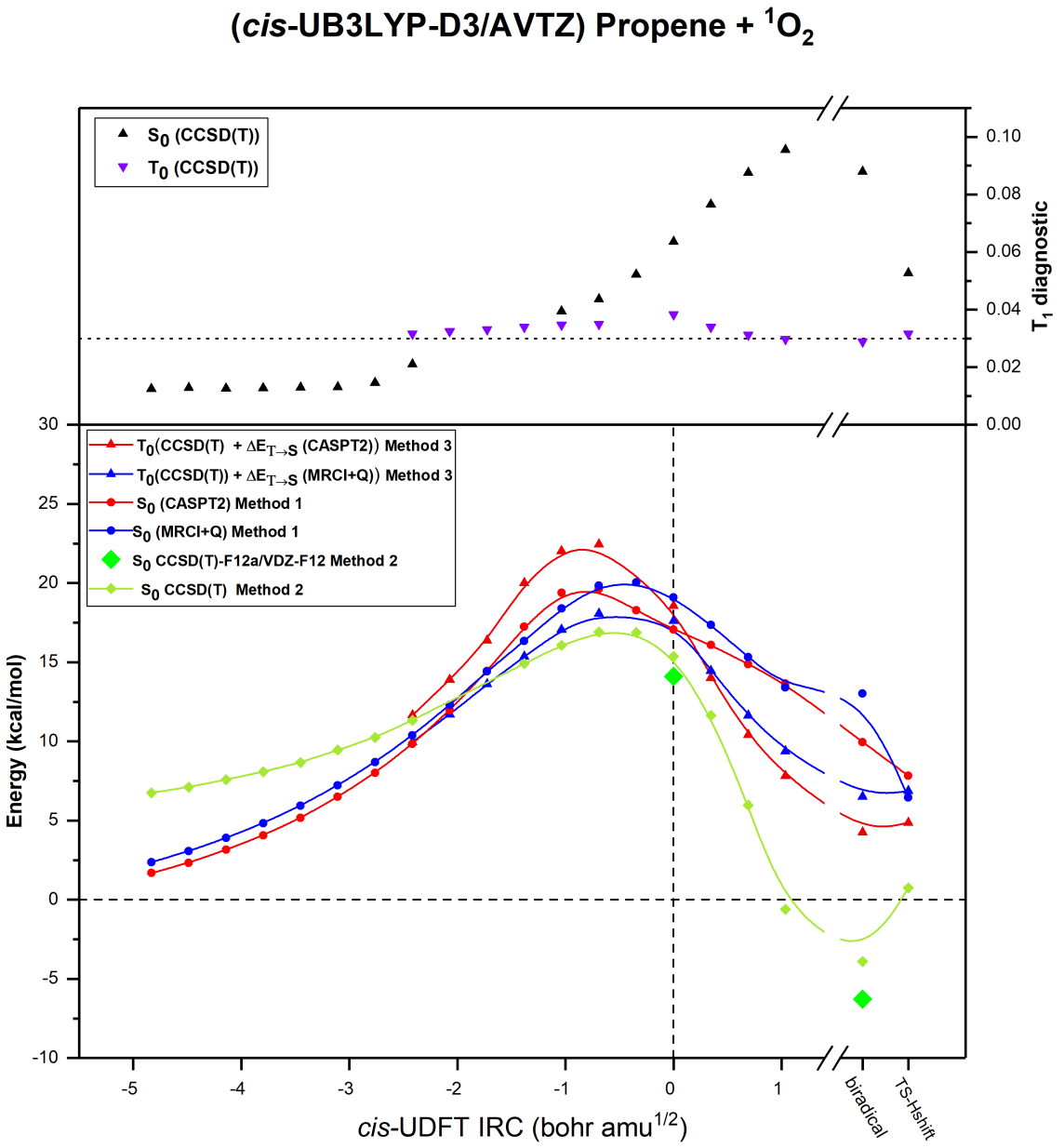

Figure 4: Lower panel Energy refinement of S_0 by method 1, 2 and 3, along the reaction coordinate for *cis*-UDFT propene. Upper panel T_1 diagnostic of S_0 and T_0 along the same reaction coordinate.

Figure 36 presents the calculated S_0 surfaces. It is observed that the T_1 diagnostic of S_0 increases in the TS and product regions to levels much higher than 0.03, which indicates that the calculations using method 2 are less reliable. On the other hand, the T_1 diagnostic of T_0 is

close to 0.03 along the entire potential energy surface. The refined energy of the *cis*-UDFT-TS varies between (14.10-19.09) kcal/mol. If calculations using method 2 are excluded, due to the high T_1 diagnostics then the refined energy of the TS is (17.06-19.09) kcal/mol. All of the refined potential energy surfaces predict an earlier TS compared to UDFT. The difference is largest for method 3, where the CASPT2/AVTZ singlet/triplet energy is added to the CCSD(T)/AVTZ triplet energy. Here the maximum of the energy surface is 22.45 kcal/mol, while the energy of the TS is only 18.56 kcal/mol. Saito et al. studied the reaction between singlet oxygen and ethene,[41] where the geometries were optimized with UDFT as well as approximate spin projection methods. Their results show that the studied UDFT methods tend to optimize TS which are more "product like" compared to the AP-UDFT method. Showing that the spin contamination error affect the geometric parameter obtained with UDFT methods. The fact that all the tested energy corrections predict an earlier TS, hints towards the spin contamination problems of the UDFT wavefunction. The spin-contamination observed for the UDFT methods mainly originate from the triplet state. In the case of the propene + singlet oxygen reaction it is expected that the spin contamination of the UDFT wave function will tend to favour the biradical path over the concerted part. When the electronic energy is refined with approximate spin projection methods, as in the work of Maranzana et al.,[13] the geometry optimization is still performed without spin projection. Hence, these calculations will inherently be affected by spin contamination via the geometry optimization. We argue that care should be taken when using the UDFT methods for geometry optimization, especially if spin-contamination is high.

cis-TS-RDFT

The T_1 diagnostics for *cis*-TS-RDFT are (0.025-0.027) which is higher than the threshold accepted for closed shell species but lower than that for open shell species. Since it is reasonable to assume that *cis*-TS-RDFT has some biradical character, a T_1 diagnostic < 0.03 is assumed to ensure the quality of the CCSD(T)-F12a/VDZ-F12 wave function. An investiga-

tion of the IRC obtained with RB3LYP-D3/AVTZ is performed similar to that for the IRC of UB3LYP-D3/AVTZ. Again, the IRC obtained from RB3LYP-D3/AVTZ is used as a general representative for the energy surfaces obtained with RDFT. The energy surfaces calculated for *cis*-TS-RDFT are shown in Figure 37. The IRC going towards the reactant region is terminated early because the reactants are too high in energy for the RDFT method, which makes the convergence of the IRC difficult. A scan was performed starting at the IRC endpoint. By extending the carbon-oxygen distance involved in bond formation by 1 Angstrom in steps of 0.1 Angstrom. As seen in Figure 37, this scan extends the potential energy surface further towards the reactant region with energies within 1 kcal/mol of the energies at 30 Angstrom separation. The energy levels of the separated reactants match the expected energy level of molecular oxygen with S_1=0.00/**0.00**/*0.00* kcal/mol, S_2=15.81/**17.60**/*15.0* kcal/mol and T_0=-21.88/-**23.56**/-*22.5* kcal/mol where normal font is MRCI+Q/AVTZ, bold is CASPT2/AVTZ and italic is obtained from the experimentally measured electronic transition in molecular oxygen.[42] The S_0 energy with the reactant moieties separated by 30 Angstrom is taken to be the zero point of energy. The reasonable agreement for the energy levels of the separated reactants validates the computational approach used in this study.

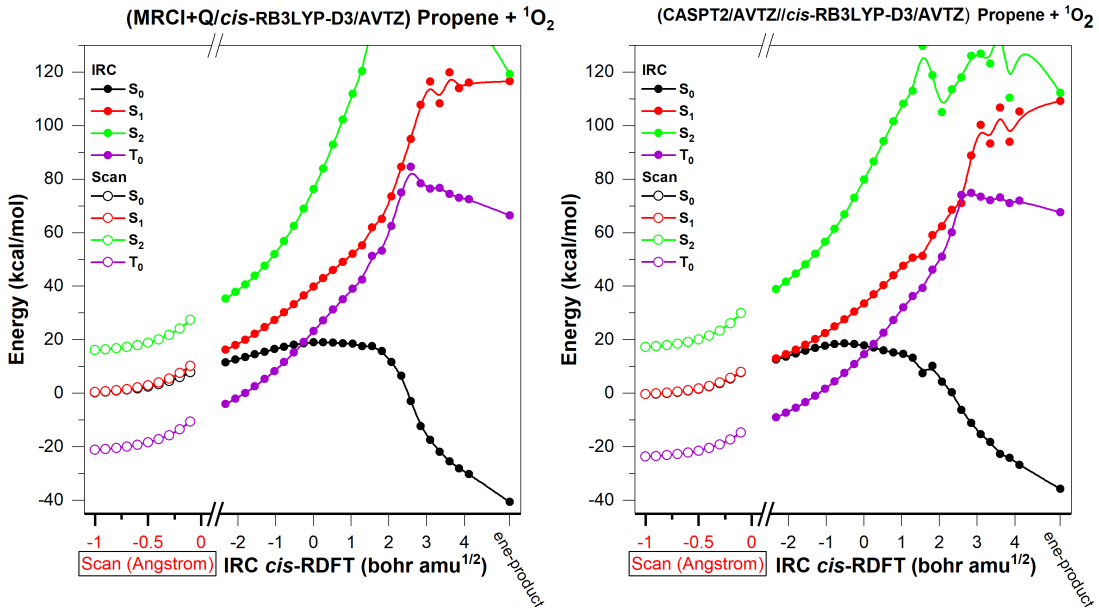

Figure 5: S_0, S_1, S_2 and T_0 electronic energy surfaces calculated by method 1 along the reaction coordinate of *cis*-RDFT.

As observed in Figure 37, the degeneracies of S_0 and S_1 are broken as the reaction proceeds from reactants to product. At the transition state the difference between S_0 and S_1 is 15.73 and 20.76 kcal/mol at the CASPT2/AVTZ and MRCI+Q/AVTZ levels of theory, respectively. The S_0 and T_0 surfaces intersect in the TS region and surface hopping at this region is a potential route for quenching the reaction, since the T_0 surface is fully repulsive at this point of the surface. Continuing along the reaction coordinate towards the product; S_0 decreases in energy while the other states increase. The energy difference between S_0 and T_0 at the IRC endpoint is around 90 kcal/mol, indicating that a single electronic state will dominate the electronic ground state and the multi-reference character of S_0 is low.

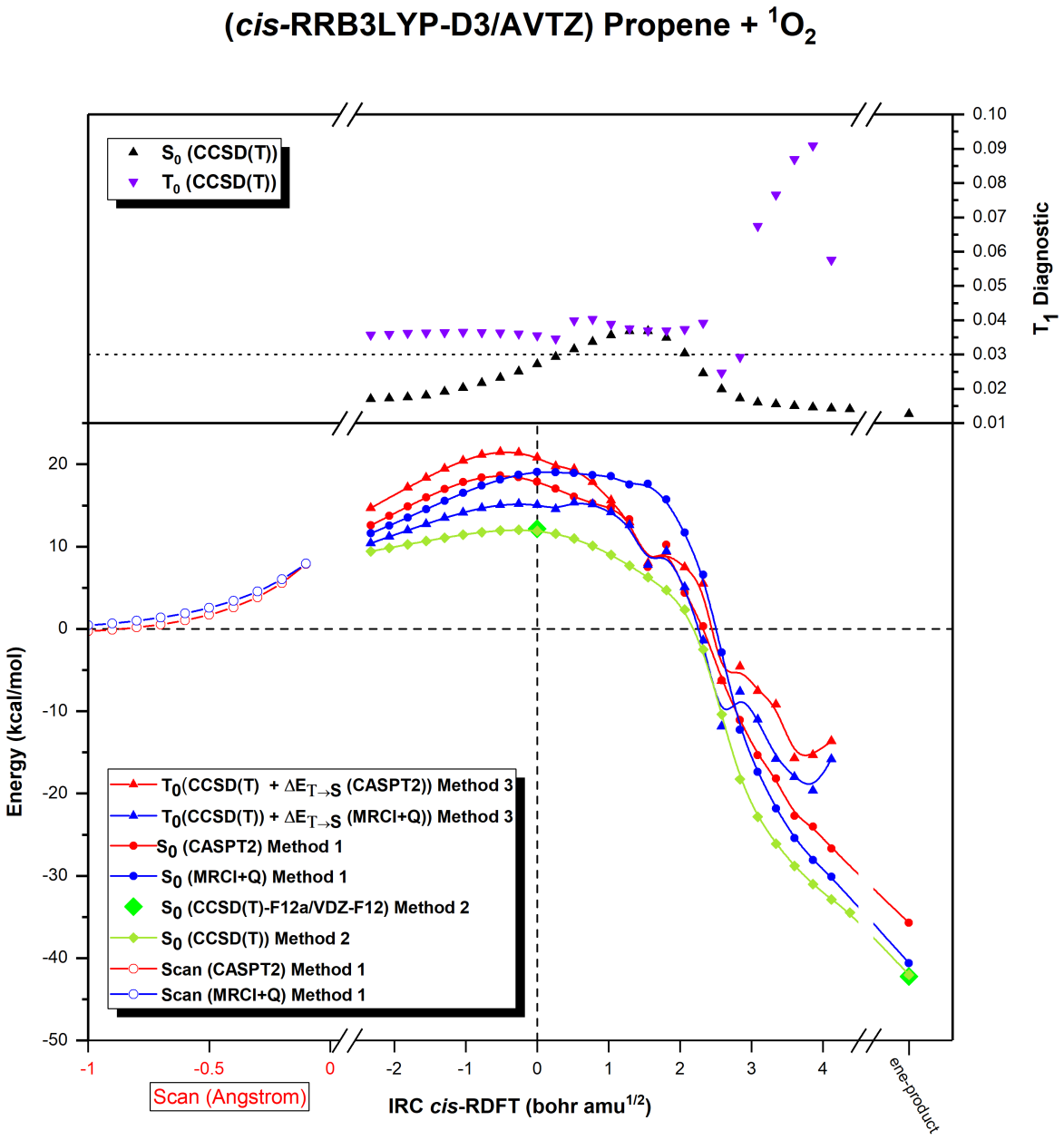

Figure 6: Lower panel Energy refinement of S_0 by method 1, 2 and 3, along the reaction coordinate for *cis*-RDFT propene. Upper panel T_1 diagnostic of S_0 and T_0 along the same reaction coordinate.

We will now focus on the S_0 surface. Figure 38 shows the energy refinement of S_0. First, we note that the T_1 diagnostics are consistently lower for S_0 than for T_0. The T_1 diagnostics for the T_0 state increase to values higher than 0.05 in the later part of the reaction

coordinate; the high value invalidates the use of CCSD(T) in this region. The high values for T_0 could be caused by the involvement of higher lying triplet states in this part of the reaction coordinate. This theory was not investigated further, but it is worth noting that even though method 3 gives an adequate description of the reactant, this result might not hold for all parts of the reaction coordinate.

The maxima of the refined potential energy surfaces for the *cis*-TS-RDFT surfaces align reasonably well with the RDFT maximum. While the CASPT2/AVTZ surface peaks slightly closer to the reactant region, indicating an earlier TS, the MRCI+Q/AVTZ surface aligns with the RDFT surface. The S_0 surface calculated using method 2 predicts a slightly earlier TS, but the energy difference between the highest energy of the S_0 surface and the energy calculated at the *cis*-TS-RDFT level is less than 1 kcal/mol, indicating the RDFT method gives a reasonable description of the reaction coordinate. Another interesting observation is that the S_0 surface calculated using CCSD(T)/AVTZ (method 2) is consistently lower than the surface calculated using CASPT2/AVTZ and MRCI+Q/AVTZ. The difference is largest in the TS region. This might indicate that higher order excitations are needed for this region to correctly describe the correlation energy. The T_1 diagnostic for S_0 becomes higher than 0.03 outside the TS region indicating that the CCSD(T)/AVTZ energies are less reliable in this region. It is seen that the more cost efficient CCSD(T)-12a/VDZ-F12 method gives energies similar to the ones obtained using CCSD(T)/AVTZ, meaning that it is possible to extend this method to larger systems. The refined energy of the *cis*-TS-RDFT surface, varies between (11.90-19.07) kcal/mol, depending of the method. The large variation across the tested methods shows the difficulties in obtaining reliable energy barriers for these types of systems.

Comparisions between *cis*-TS-RDFT and *cis*-TS-UDFT

We will address the question as to whether the concerted (*cis*-TS-RDFT) or the step wise addition mechanism (*cis*-TS-UDFT) is the lowest energy reaction path. Both surfaces are affected by multi-reference character which makes it difficult to obtain accurate energy barriers. However, when the energy maxima of the calculated PES's are compared, they all predict the RDFT to be lowest in energy by 0.94-4.89 kcal/mol which suggests that this reaction path has the lowest energy. In addition we note the indication that reaction on the (*cis*-TS-UDFT) surface might proceed via a quenching mechanism due to the closeness of the S_0 and T_0 states in the biradical intermediate. Marazana et al. calculated the energy barrier for *cis*-UDFT/AVTZ to be 12-16 kcal/mol, in good agreement with our result of 14.10-19.09 kcal/mol. However we have a different conclusion regarding the *cis*-RDFT/AVTZ results. Marazana claims the *cis*-RDFT/AVTZ result is an artefact of the RDFT method, one justification being that they were unable to find the concerted path with CASSCF optimization. We have tried to optimize the TS with CASPT2/AVTZ, but have been unable to locate the transition state with this method. However, since we performed energy refinement of the entire IRC from reactants to product, and concluded that the RDFT is the lowest energy path, we conclude that the *cis*-RDFT/AVTZ is not an artefact.

trans-Addition

We will now examine the addition of singlet oxygen *trans* to the allylic group. The *trans*-TS is not thought to follow the ene-reaction mechanism, but it might be competitive with it. Calculated $\left\langle \hat{S}^2 \right\rangle$, T_1 diagnostics, energy barriers and rate constants are shown in Table 2.

Table 2: Calculated spin contamination($\langle S^2 \rangle$), T_1 diagnostics and energy barriers calculated with CCSD(T)-F12a/VDZ-F12//DFT/AVTZ using method 2 for energy refinement (E_0) and rate constants k for the *trans*-addition of singlet oxygen to propene.

Propene + $^1O_2$ (*trans*-TS)	$\langle S^2 \rangle$	T_1	E_0 (kcal/mol)	k ($\frac{cm^3}{s}$)
RM06-2X		0.031	19.61	1.82×10^{-28}
RωB97XD		0.032	19.47	2.75×10^{-28}
RB3LYP-D3		0.039	17.57	4.81×10^{-27}
UB3LYP-D3	0.982	0.127	8.38	1.17×10^{-19}

trans-TS-UDFT

The *trans*-UDFT/AVTZ surface is highly spin-contaminated with $\left\langle \hat{S}^2 \right\rangle \approx 1$ and has a T_1 diagnostic of 0.093, which indicates a strong multi-reference character in the TS. The IRC calculated by UB3LYP-D3/AVTZ is used represent the general trend obtained with UDFT methods for this reaction path. The S_0, S_1, S_2 and T_0 surfaces are shown in Figure 40. The product of the *trans*-UDFT/AVTZ surface is a biradical intermediate where S_0 and T_0 have similar energies; and they are separated by 1.61 and 1.21 kcal/mol at the CASPT2/AVTZ and MRCI+Q/AVTZ levels of theory respectively. This reaction path will likely lead to quenching back to the triplet state, and it is seen that the *trans*-UDFT/AVTZ result is similar to the *cis*-UDFT/AVTZ. Marazana studied the formation of dioxetane from the biradical intermediates and found that the ene-product was favoured over the dioxetane by a factor of 3000, hence this reaction path was not studied further. Although, assuming the dioxetane formed from the biradical is connected by an energy barrier, it is reasonable to suggest that quenching will be the most likely outcome for such a reaction. The refined S_0 surface of *trans*-UDFT/AVTZ is shown in Figure 39. The T_1 diagnostic for S_0 is very high and while it is lower for T_0. The consequence of the high T_1 diagnostic is a much lower energy for the biradical product, which is an artefact of the poor quality of the CCSD(T) wavefunction. The energy of the *trans*-UDFT-TS is 8.10-20.84 kcal/mol, or 18.90-20.84 kcal/mol when excluding the unreliable results for S_0 from CCSD(T). Once again, energy refinement predicts an earlier TS compared to UDFT, which increases the energy barrier of

the reaction to 20.29-23.43 kcal/mol after energy refinement. The tested methods predict the energy barrier for the *trans*-UDFT/AVTZ path to be higher for *cis*-UDFT/AVTZ by 0.88-2.65 kcal/mol, indicating that the addition *cis* to the methyl group is preferred over *trans*-addition.

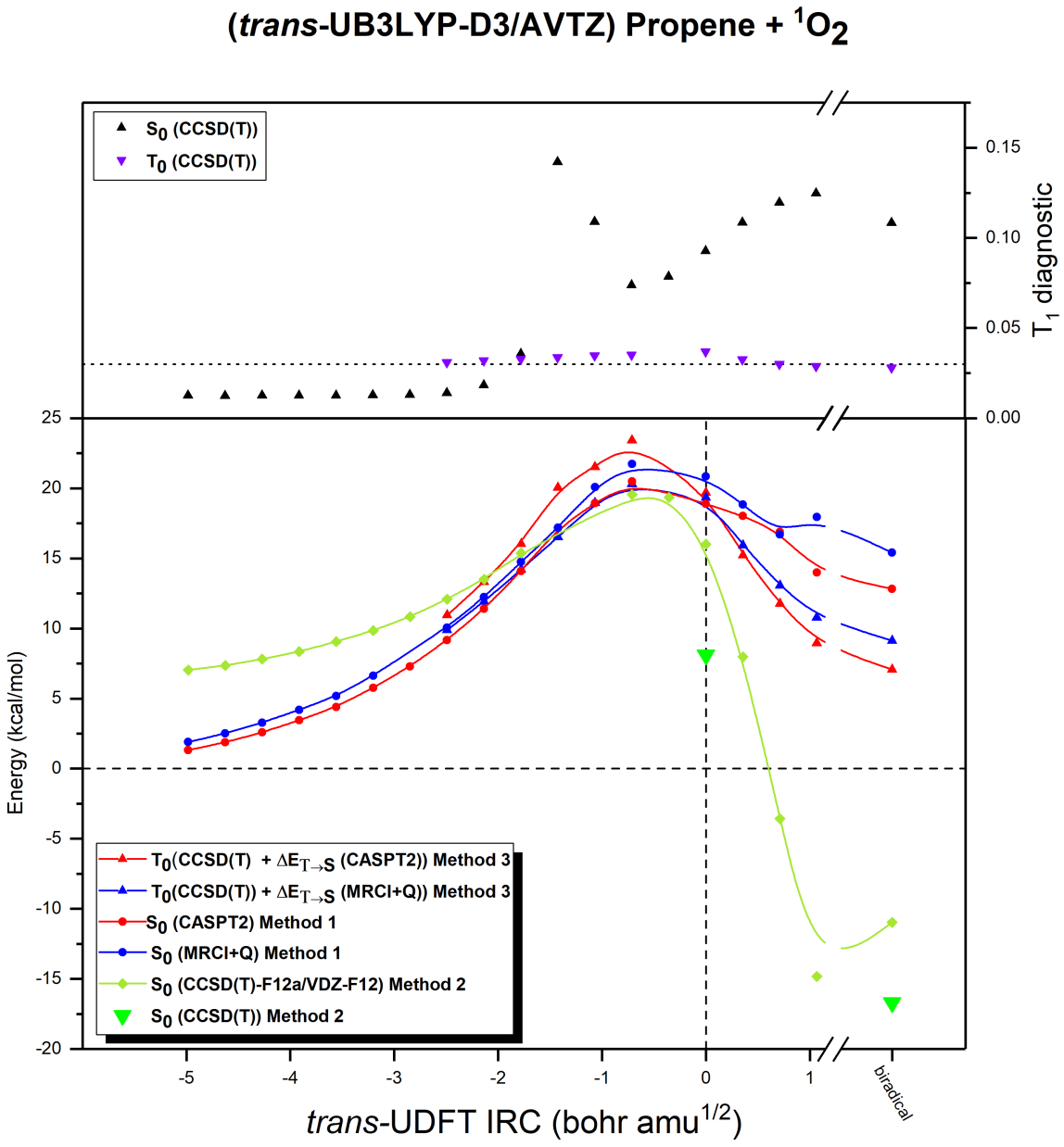

Figure 7: Lower panel Energy refinement of S_0 by method 1, 2 and 3, along the reaction coordinate for *trans*-TS-UDFT propene. Upper panel T_1 diagnostic of S_0 and T_0 along the same reaction coordinate.

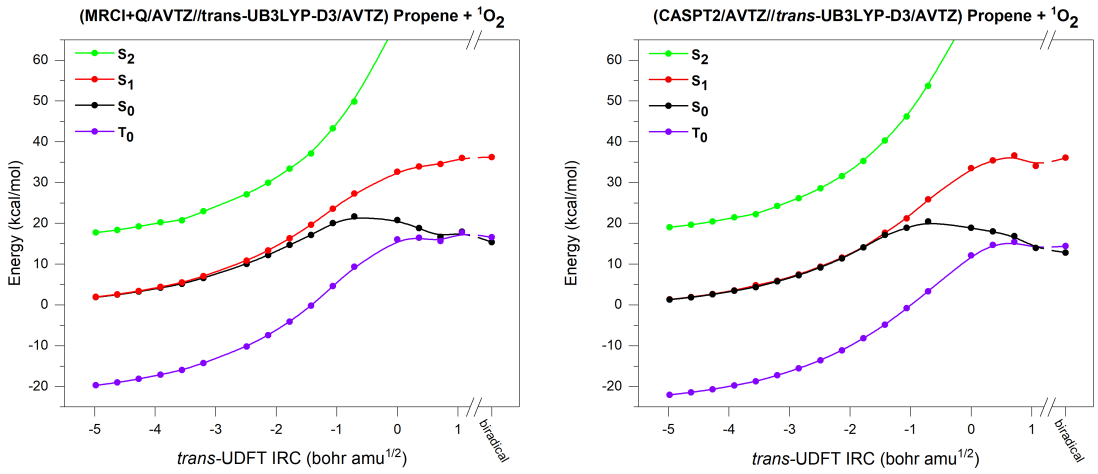

Figure 8: S_0, S_1, S_2 and T_0 electronic energy surfaces calculated by method 1 along the reaction coordinate of *trans*-UDFT.

trans-TS-RDFT

Figure 41 presents the refined energy surface for the *trans*-RDFT/AVTZ reaction coordinate. S_0 increases from reactants to the TS and decreases from the TS to product while S_1, S_2 and T_0 increase in energy from reactants to product, resulting in a well separated S_0 state in the product region. The T_0 and S_0 surfaces intersect before the TS.

Figure 42 shows the S_0 surface after energy refinement for the *trans*-RDFT/AVTZ reaction coordinate. The T_1 diagnostic for S_0 has a very similar shape to the one observed for the *cis*-RDFT/AVTZ surface. In Figure 38, as it starts low and increases more than 0.03 in the region around and after the TS. The T_1 diagnostic of T_0 is near or just above 0.03 over the entire surface. The S_0 potential energy surface has two bumps which can be understood when looking at the TS structure in Figure 34. The bond between oxygen and the central carbon is formed first, followed by bond formation to the outer carbon atom, showing that the reaction occurs asynchronously. Interestingly, this asynchronous addition leads to two energy maxima along the CASPT2/AVTZ (method 1) and CCSD(T)/AVTZ+CAPT2/AVTZ (method 3) surfaces and therefore a second TS is predicted by these methods. We have not

been able to locate a second transition state for the second C-O bond formation with the tested DFT functionals. The energy of the perepoxide product varies between 5-19 kcal/mol. The large variation between the methods for the perepoxide product is surprising since the surface should not have significant multi-reference character, which is reflected in the low T_1 diagnostic of the perepoxide. The variation might be due to insufficient inclusion by dynamic correlation of the CASPT2 and MRCI+Q methods. Furthermore, Marazana et al. found the perepoxide to be 19.5 kcal/mol higher than the isolated reactants in excellent agreement with the values we obtain using the CASPT2/AVTZ method. However, some of the key conclusions in that paper arise from the perepoxide being located approximately 12 kcal/mol higher than the biradical. The MRCI+Q method predicts that the perepoxide is located 5.59 and 3.22 kcal/mol lower in energy than, respectively, the *trans*-biradical and *cis*-biradical.

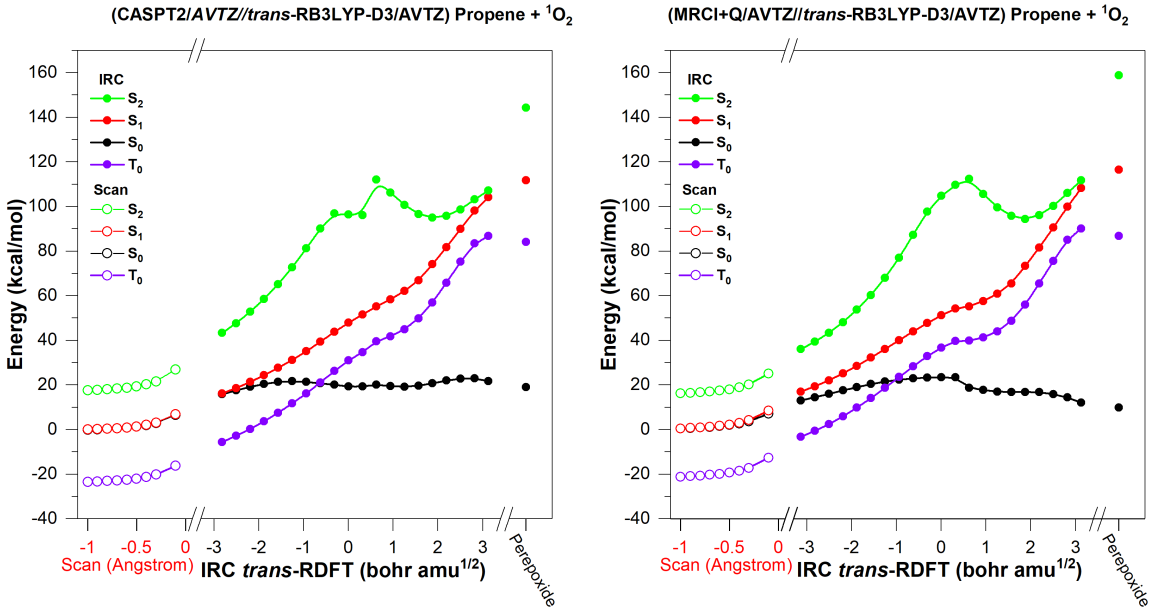

Figure 9: S_0, S_1, S_2 and T_0 electronic energy surfaces calculated by method 1 along the reaction coordinate of *trans*-RDFT.

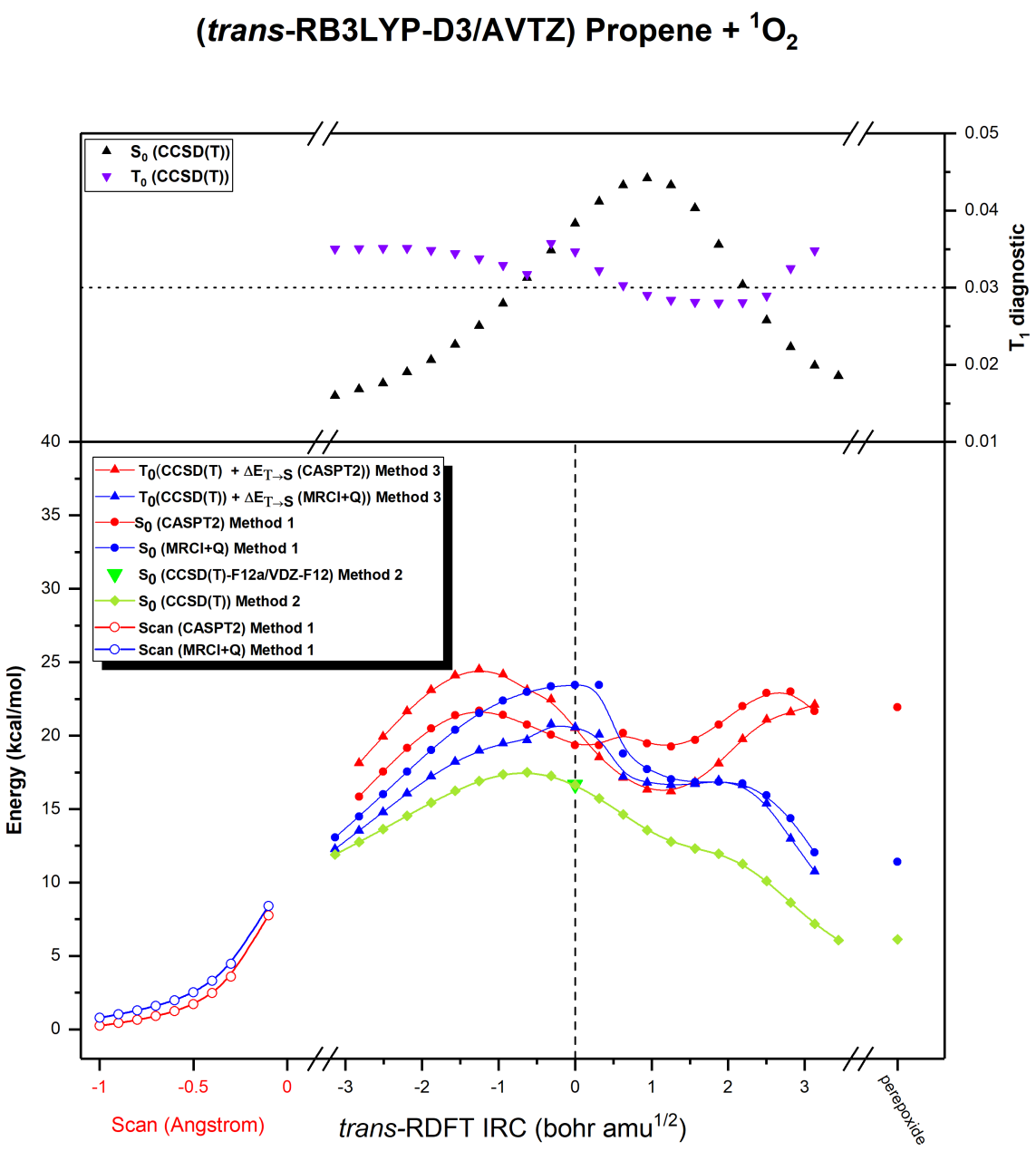

Figure 10: Lower panel Energy refinement of S_0 by method 1, 2 and 3, along the reaction coordinate for *trans*-RDFT propene. Upper panel T_1 diagnostic of S_0 and T_0 along the same reaction coordinate.

2-methylpropene

To our knowledge there have been no other studies of the reaction between 2-methylpropene and singlet oxygen. This system plays an important role in the current work, since it is part of the gradual methyl substitution of propene that constitutes our testing system, and the results for this system should align with any qualitative trends in the reactivity of singlet oxygen with the methyl-substituted alkenes. The symmetry of the 2-methylpropene reaction means that addition on either side of the double bond is identical.

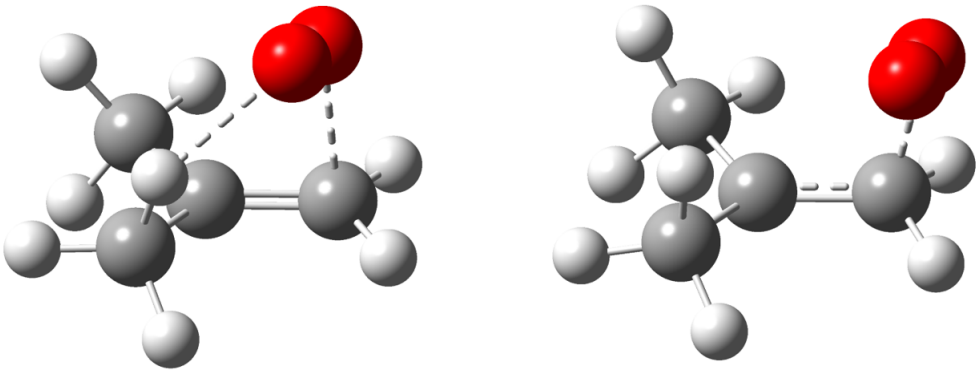

Figure 11: TS structure of TS-RDFT (left) and TS-UDFT (right), calculated at the (R/U)B3LYP-D3/AVTZ level of theory.

The optimized structure for the B3LYP-D3/AVTZ calculation is shown in Figure 43 and represents the general features of the UDFT and RDFT optimizations. The UDFT optimizations predict a stepwise addition forming a biradical/zwitterionic intermediate, whereas the RDFT calculations predict a concerted reaction that forms the hydroperoxide in one step. $\langle S^2 \rangle$, T_1, refined energy barriers and rate constants are shown in Table 3. The $\langle S^2 \rangle$ for the TS-UDFT wave-function (0.925-1.003) shows strong spin contamination and the T_1 diagnostic of (0.071-0.092) indicates that multi-reference character is pronounced for TS-UDFT therefore requiring multi-reference treatment. The TS-RDFT has a T_1 diagnostic (0.025-0.027) that is similar that obtained for the propene system justifying the use of single reference methods for this TS. The energy barrier for the formation of TS-RDFT is (11.56-11.74) kcal/mol calculated after CCSD(T)-F12a/VDZ-F12 refinement, while it is (12.76-15.55) kcal/mol for

Table 3: Calculated spin contamination($\langle S^2 \rangle$), T_1 diagnostic and energy barriers calculated at the CCSD(T)-F12a/VDZ-F12//DFT/AVTZ level of theory using method 2 for energy refinement (E_0) and rate constants k.

2-methylpropene+ $^1O_2$	$\langle S^2 \rangle$	T_1	E_0 (kcal/mol)	k ($\frac{cm^3}{s}$)
RM06-2X		0.025	11.58	1.20×10^{-22}
RM06-2X*		0.025	11.58	1.23×10^{-22}
RωB97XD		0.025	11.74	7.54×10^{-23}
RωB97XD*		0.025	11.73	7.61×10^{-23}
RB3LYP-D3		0.027	11.56	1.10×10^{-22}
UM06-2X	0.989	0.071	15.55	8.84×10^{-25}
UωB97XD	1.003	0.092	13.89	2.05×10^{-23}
UB3LYP-D3	0.925	0.071	12.76	7.21×10^{-23}

$*$: The geometry optimization was performed using the superfine grid.

the TS-UDFT.

We now focus on the energy refinement of the IRC obtained with the RB3LYP-D3/AVTZ and UB3LYP-D3/AVTZ methods. The results from this energy refinement are used to present general features of the optimization with the UDFT and RDFT methods. All energy refinements along the reaction coordinate are done with the AVTZ basis set, to eliminate any basis set effect of this investigation.

RDFT-TS

Figure 44 shows the CASPT2/AVTZ and MRCI+Q/AVTZ energy refinements for S_0, S_1, S_2 and T_0 along the IRC obtained with RB3LYP-D3/AVTZ. S_1, S_2 and T_0 increase in energy along the reaction coordinate and reach values much higher than S_0 in the product region.

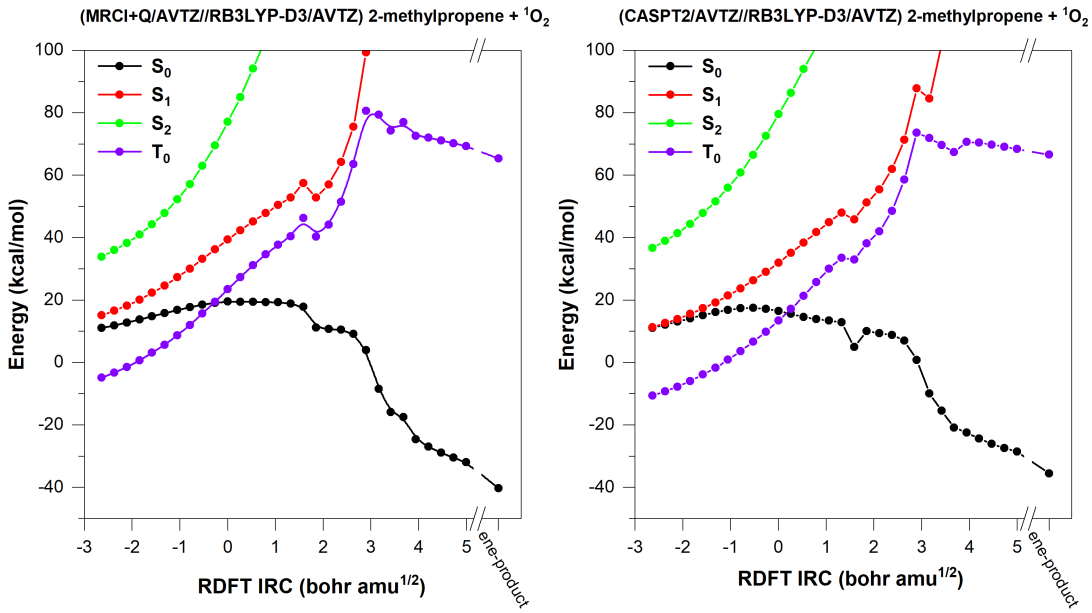

Figure 12: S_0, S_1, S_2 and T_0 electronic energy surfaces calculated by method 1 along the reaction coordinate of TS-RDFT

The S_0 and T_0 surfaces intersect close to the RDFT-TS. The S_0 surface refined by methods 1, 2 and 3 is shown in Figure 13. The T_1 diagnostic for S_0 increases above 0.03 after the RDFT-TS indicating the limited accuracy of CCSD(T) for this part of the potential energy surface. The T_1 diagnostic of T_0 lies above 0.03 for the entire potential energy surface, and seems to increase towards the product region. The refined energy of the RDFT-TS is 16.51 (CASPT2/AVTZ method 1), 19.51 (MRCI+Q/AVTZ method 1), 10.39 (CCSD(T)/AVTZ method 2), 19.39 (CCSD(T)/AVTZ+CAPT2/AVTZ method 3) and 14.28 kcal/mol (CCSD(T)/AVTZ+(MRCI+Q/AVTZ) method 3), Method 2 predicts the lowest energy barrier for the reaction, and since the T_1 diagnostic is reasonably low for the RDFT-TS, it might indicate that higher order excitation is important to accurately describe the correlation energy in the TS region. Most of the surfaces obtained after energy refinement predicts a slightly earlier TS, which increases the energy barrier for these surfaces to 17.52 (CASPT2/AVTZ method 1), 10.55 (CCSD(T)/AVTZ method 2), 20.41 kcal/mol (CCSD(T)/AVTZ+CAPT2/AVTZ method 3). The maximum of the MRCI+Q/AVTZ energy surface aligns with the RDFT TS, while CCSD(T)/AVTZ+(MRCI+Q/AVTZ) (method

3) predicts a slightly later TS which has a maximum value of 14.68 kcal/mol. The difference between the refined energies at the optimized RDFT-TS compared to their maximum along the reaction coordinate is about 1 kcal/mol, which indicates a reasonable quality for the RDFT optimized geometries.

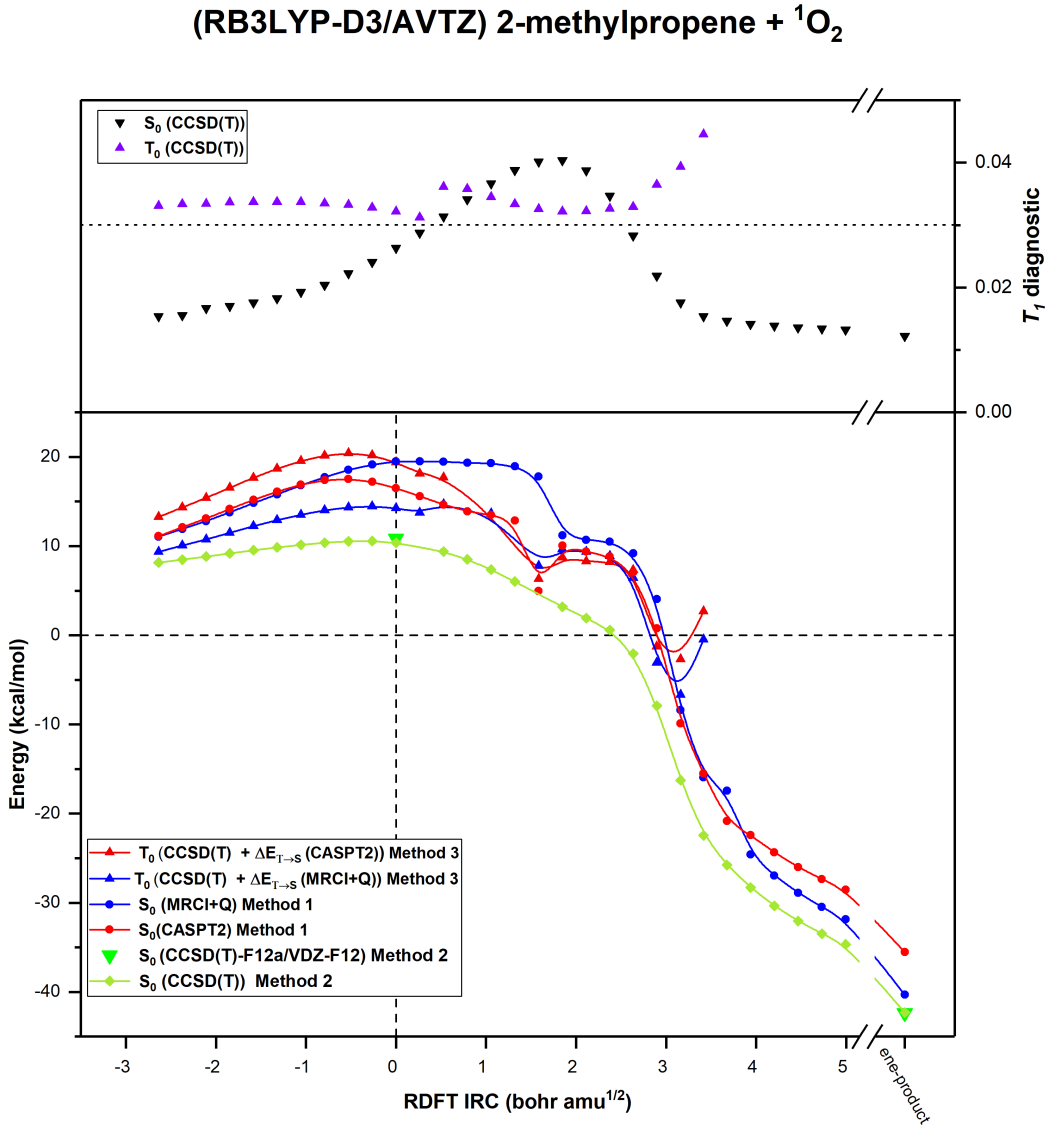

Figure 13: Lower panel Energy refinement of S_0 by method 1, 2 and 3, along the reaction coordinate for TS-RDFT. Upper panel T_1 diagnostic of S_0 and T_0 along the same reaction coordinate.

UDFT-TS

Figure 14 shows S_0, S_1, S_2 and T_0 calculated using the CASPT2/AVTZ and MRCI+Q/AVTZ methods for the reaction coordinate obtained with the UB3LYP-D3/AVTZ method. The S_0 and S_1 states remain close in energy along the reaction coordinate and are separated by 13.51 (CASPT2/AVTZ) and 11.36 (MRCI+Q/AVTZ) kcal/mol at the UDFT-TS level. We note that the S_0 and T_0 states have similar energies from the UDFT-TS towards the product region. The small energy separation between S_0 and T_0 in this part of the potential energy surface indicates that quenching back to the triplet ground state could be important for this reaction channel. The refined S_0 energies for the UB3LYP-D3/AVTZ IRC are shown in Figure 15. The energy refinement indicates the presence of an earlier TS, which again agrees perfectly with the result of Saito et al.[41] The T_1 diagnostic becomes high for S_0 around the UDFT-TS and towards the product region whereas the T_1 diagnostic of T_0 is stable around 0.03 for the entire surface. The refined energies at the UDFT-TS are 16.21 (CASPT2/AVTZ method 1), 19.61 (MRCI+Q/AVTZ method 1), 13.89 (CCSD(T)/AVTZ method 2), 17.44 (CCSD(T)/AVTZ+CAPT2/AVTZ method 3) and 16.90 kcal/mol (CCSD(T)/AVTZ+(MRCI+Q/AVTZ) method 3). As noted earlier, all the methods predict an earlier TS which increases the barrier of the refined energy surfaces to: 18.91 (CASPT2/AVTZ method 1), 20.48 (MRCI+Q/AVTZ method 1), 15.52 (CCSD(T)/AVTZ method 2), 21.77 (CCSD(T)/AVTZ+CAPT2/AVTZ method 3) and 17.45 kcal/mol (CCSD(T)/AVTZ+(MRCI+Q/AVTZ) method 3). The energy difference between the energy at the UDFT-TS and the maximum along the reaction coordinate is (0.87-4.33) kcal/mol. The large energy difference for some of the energy refinements shows the large effect of spin contamination for the obtained UDFT structures. The maximum of the refined energy for the UDFT-TS reaction coordinate is (0.97-4.97) kcal/mol higher than that of the RDFT-TS reaction coordinate. The results show that the concerted pathway is favoured but the small energy difference between the two reaction paths means they will be competitive, and might exchange if, for instance solvent effects stabilize the step wise addition more than

the concerted path.

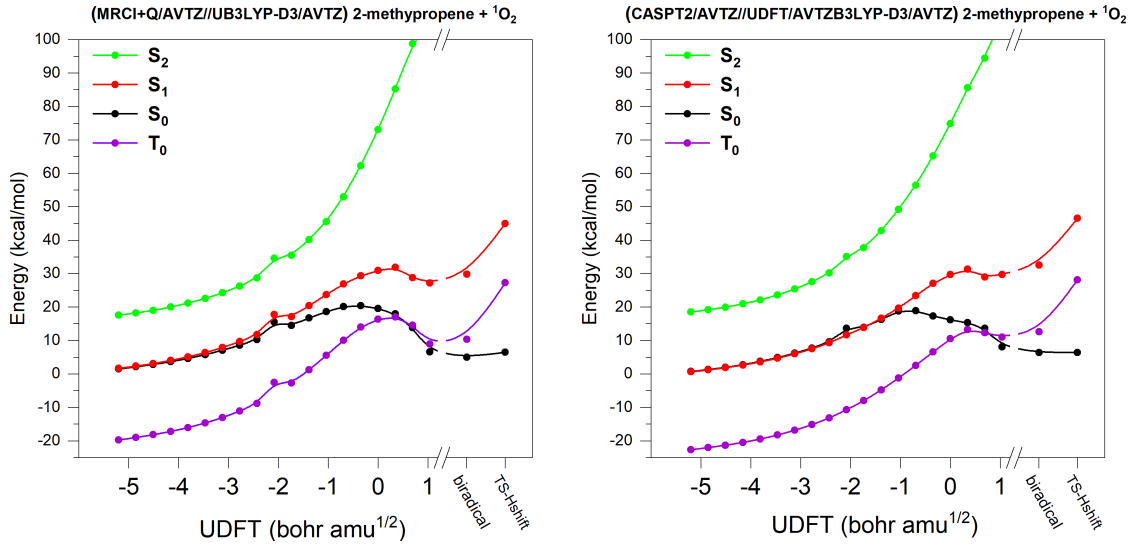

Figure 14: S_0, S_1, S_2 and T_0 electronic energy surfaces calculated by method 1 along the reaction coordinate of TS-UDFT.

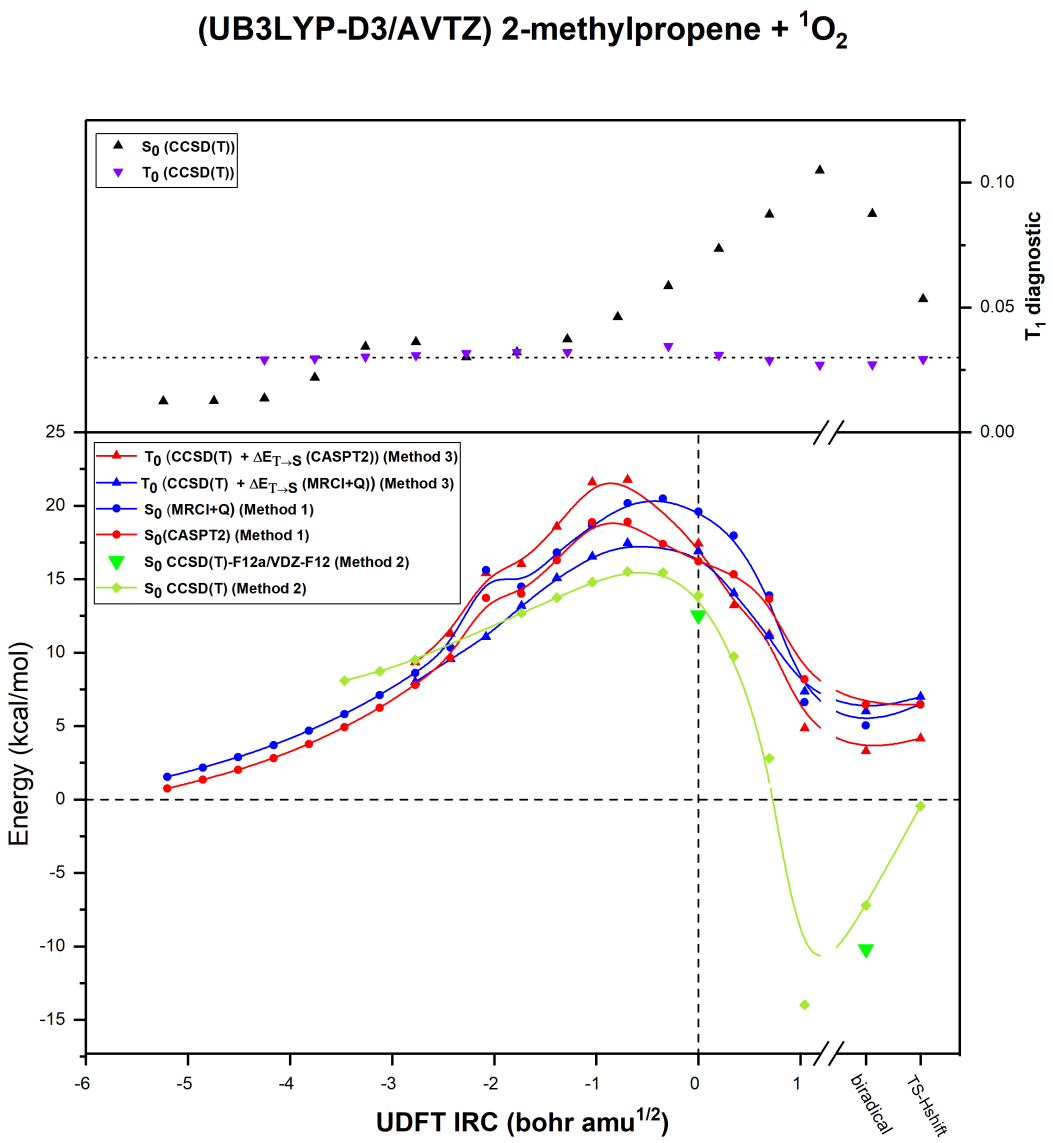

Figure 15: Lower panel Energy refinement of S_0 by method 1, 2 and 3, along the reaction coordinate for TS-UDFT. Upper panel T_1 diagnostic of S_0 and T_0 along the same reaction coordinate.

trans-butene

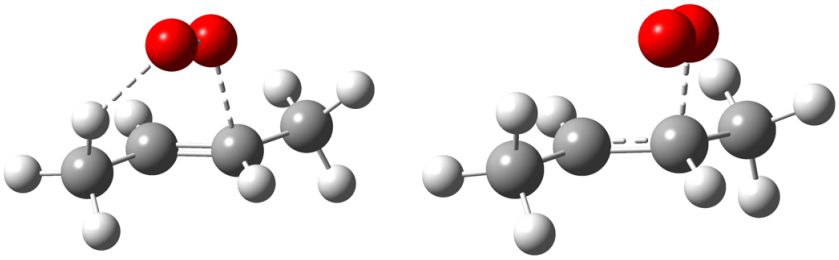

Figure 16: TS structures of TS-RDFT (left) and TS-UDFT (right) calculated at the (R/U)B3LYP-D3/AVTZ level of theory.

The *trans*-butene reaction, as for 2-methylpropene, is symmetrical with respect to singlet oxygen addition to either side of the double bond. The optimized TS structures are shown in Figure 16. The calculated energy barriers, $\left\langle \hat{S}^2 \right\rangle$, T_1 diagnostics and rate constants for the TS optimized in our calculations are shown in Table 4.

Table 4: Calculated spin contamination($\langle S^2 \rangle$), T_1 diagnostics and energy barriers calculated using CCSD(T)-F12a/VDZ-F12//DFT/AVTZ and method 2 for energy refinement (E_0) and rate constants k.

trans-butene+ $^1O_2$	$\left\langle \hat{S}^2 \right\rangle$	T_1	E_0 (kcal/mol)	k ($\frac{cm^3}{s}$)
RM06-2X		0.022	9.94	1.60×10^{-21}
RM06-2X*		0.022	9.93	1.58×10^{-21}
RωB97XD		0.024	10.00	1.20×10^{-21}
RωB97XD*		0.024	10.00	1.19×10^{-21}
RB3LYP-D3		0.024	9.85	1.74×10^{-21}
RB3LYP-D3†		0.024	9.36	4.01×10^{-21}
UM06-2X	0.959	0.052	14.02	5.80×10^{-24}
UωB97XD	0.975	0.059	14.13	5.45×10^{-24}
UB3LYP-D3	0.886	0.055	11.63	2.25×10^{-22}
exp.[43]				1.49×10^{-18}

$*$: The geometry optimization was performed using the superfine grid.
†: Energy refined at the CCSD(T)/AVTZ level.

The TS optimized with the RDFT method (TS-RDFT) follows a concerted reaction mechanism where hydrogen abstraction and oxygen addition occur simultaneously. The energy barrier is determined to be (9.85-10.00) kcal/mol after CCSD(T)-F12a/VDZ-F12

energy refinement. The TS-UDFT predicts a stepwise addition where a biradical/zwitterionic intermediate is formed followed by hydrogen abstraction forming the hydroperoxide product. The TS-UDFT wave-function is highly spin contaminated with $\left\langle \hat{S}^2 \right\rangle$ in the range of (0.886-0.975). The spin contamination likely leads to an overestimation of the biradical character of the UDFT reaction path. The energy of TS-UDFT is calculated to be (11.63-14.13) kcal/mol after CCSD(T)-F12a/VDZ-F12 energy refinement. The refined energy barriers changed by 0.15 kcal/mol across the RDFT/AVTZ methods, while the variation is 2.39 kcal/mol for the UDFT/AVTZ energy barriers. This illustrates the fact that the bypassing scheme becomes much more sensitive/unreliable for systems with high spin contamination and T_1 diagnostics.

TS-RDFT

We use the IRC obtained with (U/R)B3LYP-D3/AVTZ to further investigate the reaction coordinate.

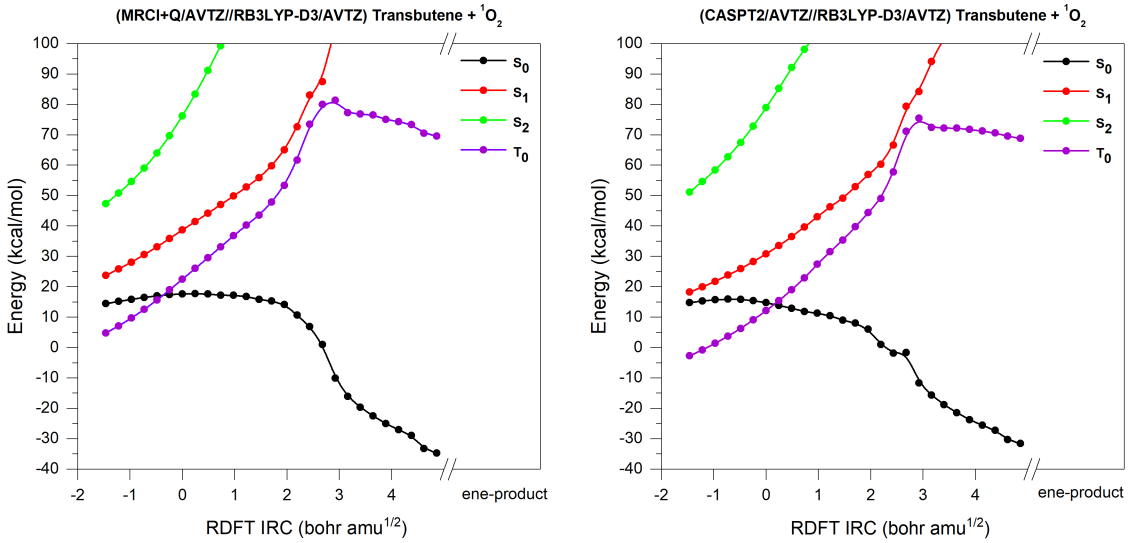

Figure 17: S_0, S_1, S_2 and T_0 electronic energy surfaces calculated by method 1 along the reaction coordinate of TS-RDFT.

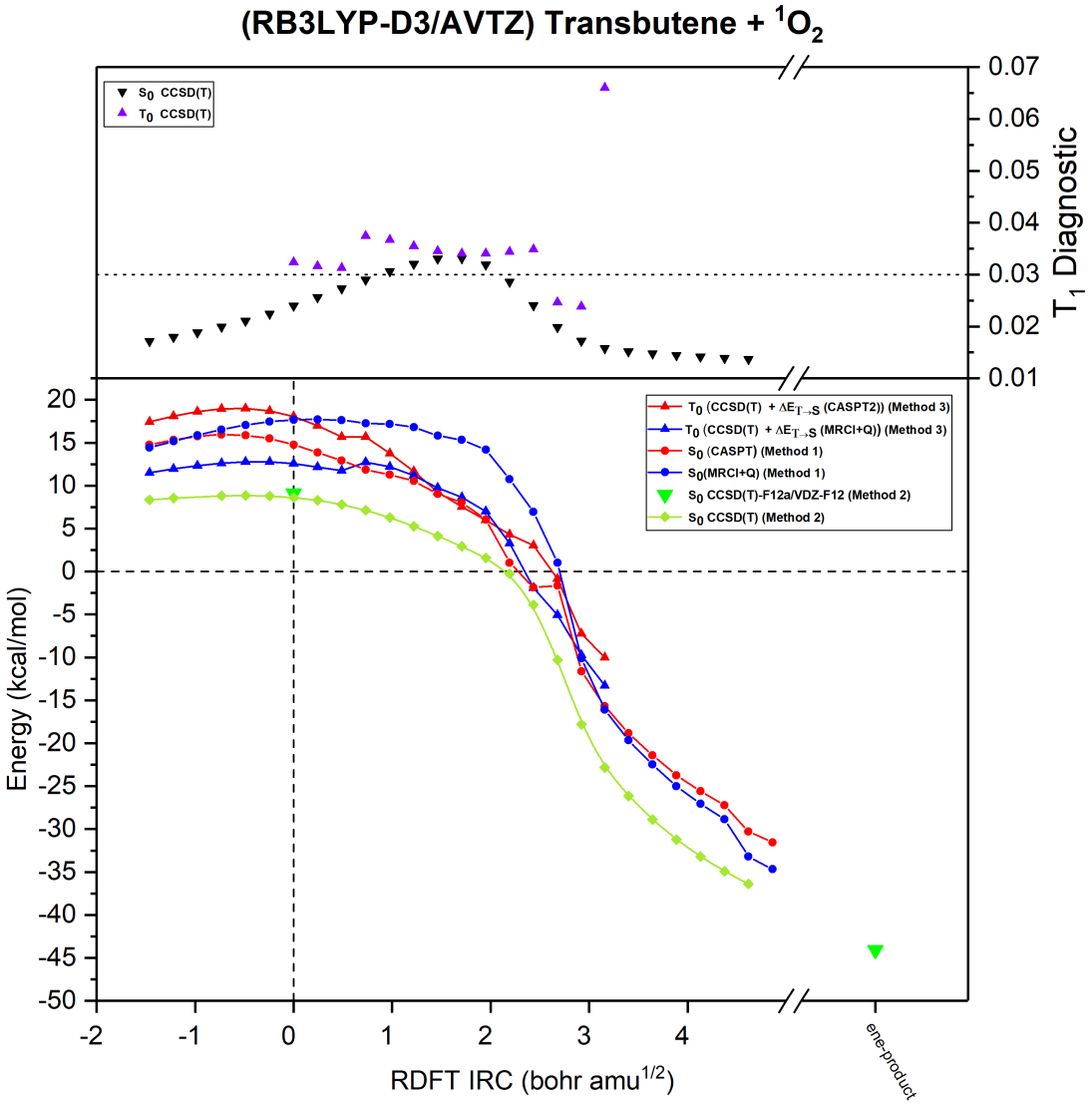

Figure 18: Lower panel Energy refinement of S_0 by method 1, 2 and 3, along the reaction coordinate for TS-RDFT. Upper panel T_1 diagnostic of S_0 and T_0 along the same reaction coordinate.

Figure 17 shows S_0, S_1, S_2 and T_0 calculated using CASPT2/AVTZ and MRCI+Q/AVTZ for the IRC obtained with the RB3LYP-D3/AVTZ method. The results show that S_0 and T_0 intersect close to the TS, while S_1 drifts away from S_0 along the reaction coordinate. At the TS the energy difference is 16.09 kcal/mol with CASPT2/AVTZ (method 1) and 21.07

kcal/mol with MRCI+Q/AVTZ (method 1), which clearly shows that the initial degeneracy of S_0 and S_1 is lost in the TS and in addition that the the multi-reference character of the TS might be lower compared to that of the reactants. In the product region there is sufficient energy difference between S_0 and the other excited electronic states, hence single reference methods are expected to yield reliable results for S_0. Figure 17 shows S_0 for the reaction coordinate obtained with RB3LYP3-D3/AVTZ after energy refinement. The T_1 diagnostic for S_0 is lower than 0.03 for most of the reaction coordinate, but reaches the maximum value of 0.033 between the TS and product. The refined energy of the RDFT-TS is 14.77 CASPT2/AVTZ (method 1), 17.68 MRCI+Q/AVTZ (method 1), 8.62 CCSD(T)/AVTZ (method 2), 18.03 CCSD(T)/AVTZ+CAPT2/AVTZ (method 3) and 12.55 kcal/mol CCSD(T)/AVTZ+(MRCI+Q/AVTZ) (method 3). The refined energies of the TS vary by about 10 kcal/mol across the tested methods. This variation is similar to those observed for propene and 2-methylpropene. Most of the energy refinements indicate a slightly earlier TS, with the exception being MRCI+Q/AVTZ which predicts a slightly later TS. The energy differences for the maximum on the refined reaction coordinate compared to the energy of the RDFT-TS is (0.04-1.18) kcal/mol which indicates a fairly good quality for the RB3LYP-D3/AVTZ geometry.

TS-UDFT

Figure 19 shows S_0, S_1, S_2 and T_0 calculated using CASPT2/AVTZ and MRCI+Q/AVTZ for the reaction coordinate obtained with the UB3LYP-D3/AVTZ method. The surfaces S_0, S_1 and T_0 remain energetically close along the reaction coordinate. The energy difference between S_0 and T_0 is only 4.05 (CASPT2/AVTZ) and 1.24 kcal/mol (MRCI+Q/AVTZ) at the TS while the differences between S_0 and S_1 are 15.77 (CASPT2/AVTZ) and 14.07 kcak/mol (MRCI+Q/AVTZ). The similarity of the energies of S_0 and T_0 along the reaction coordinate indicates that quenching back to the triplet state might be important for this reaction path.

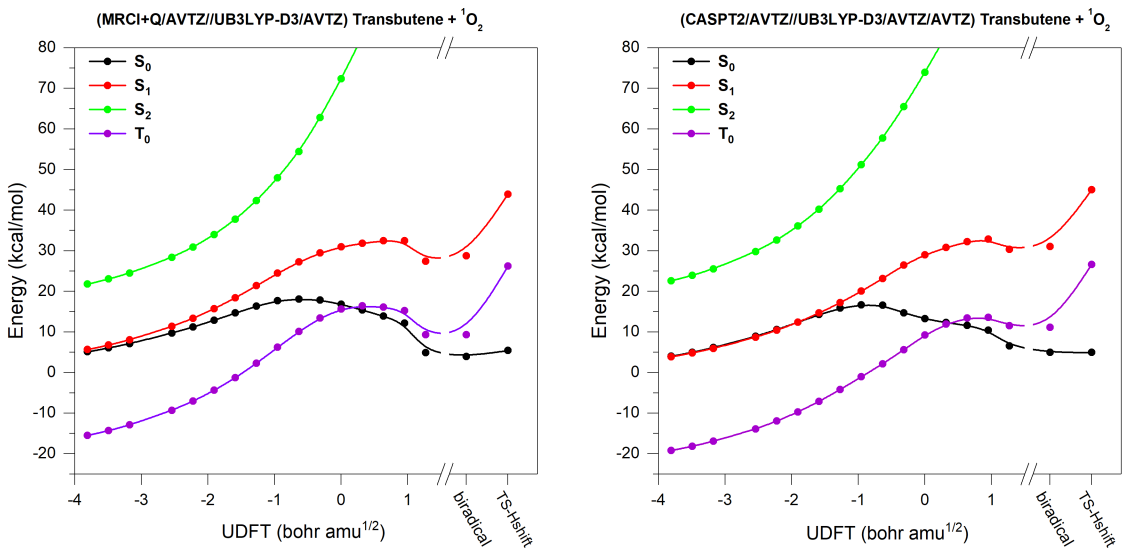

Figure 19: S_0, S_1, S_2 and T_0 electronic energy surfaces calculated by method 1 along the reaction coordinate of TS-UDFT.

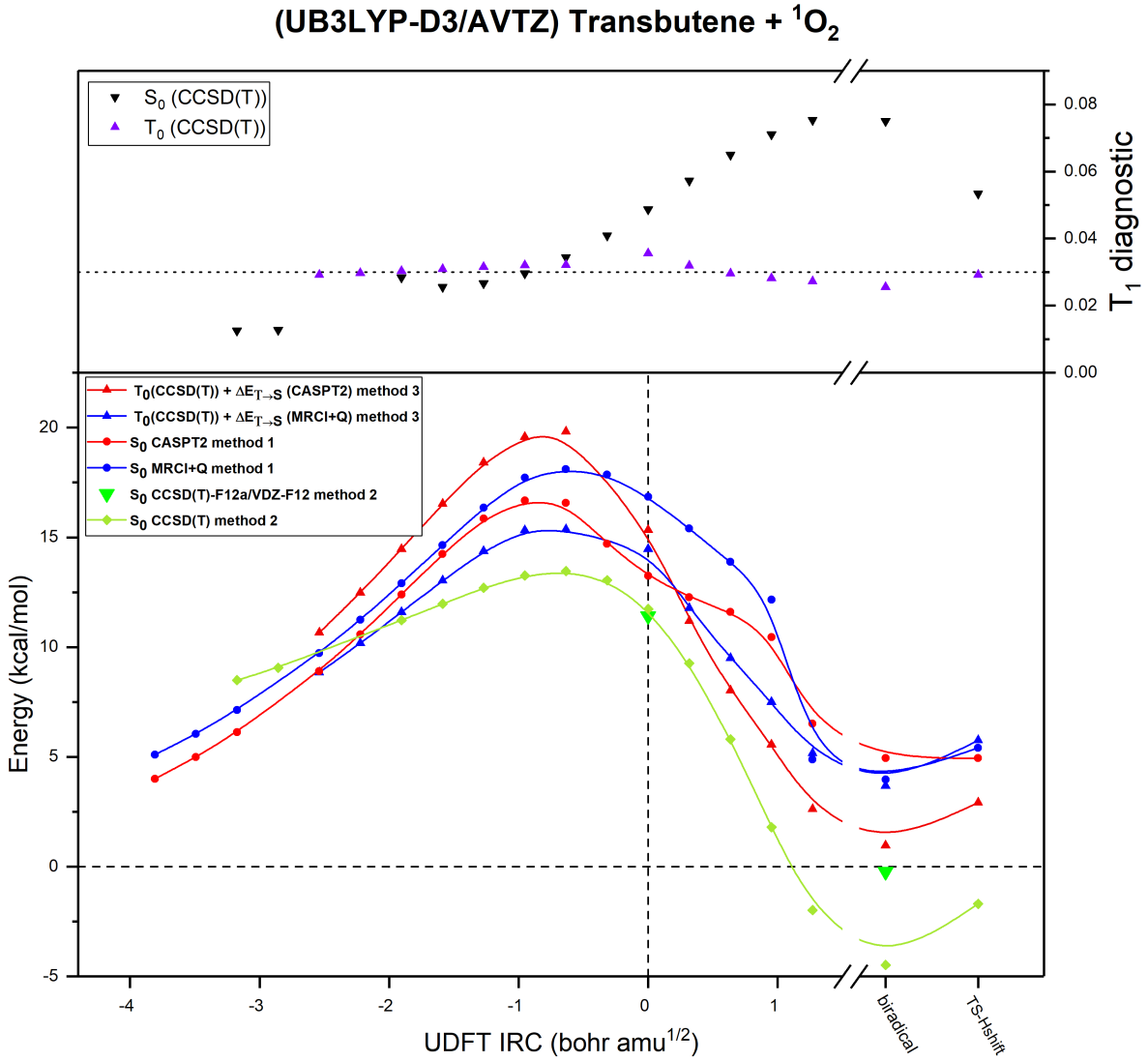

Figure 20: Lower panel Energy refinement of S_0 by method 1, 2 and 3, along the reaction coordinate for TS-UDFT. Upper panel T_1 diagnostic of S_0 and T_0 along the same reaction coordinate.

Figure 20 shows the refined energies of S_0 for the UDFT-TS reaction coordinate. All the energy refinements indicate an earlier TS, similar to the results for propene and 2-methylpropene. The refined energy of the UDFT-TS is 13.24 CASPT2/AVTZ (method 1), 16.84 MRCI+Q/AVTZ (method 1), 11.74 CCSD(T)/AVTZ (method 2), 15.34 CCSD(T)/AVTZ+

CASPT2/AVTZ (method 3) and 14.46 kcal/mol CCSD(T)/AVTZ+(MRCI+Q/AVTZ) (method 3) whereas the maximum of the refined energy surface is found to be 16.67 CASPT2/AVTZ (method 1), 18.11 MRCI+Q/AVTZ (method 1), 13.46 CCSD(T)/AVTZ (method 2), 19.82 CCSD(T)/AVTZ+CAPT2/AVTZ (method 3) and 15.37 kcal/mol CCSD(T)/AVTZ+(MRCI +Q/AVTZ) (method 3). When comparing the maximum for the refined (R/U)B3LYP-D3/AVTZ reaction coordinates, RDFT is consistently found to be lower than the UDFT pathway by (0.39-4.60) kcal/mol, which shows that the RDFT is the lowest energy pathway. However the similar energies of the two reaction paths means they will be in close competition.

Ashford et al. determined the rate constant for the reaction between singlet oxygen and *trans*-butene in the gas phase form experiment.[43] This type of information is useful to validate the modelled TS and the energy refinement of the reaction coordinate. The concerted reaction path predicted by RDFT is found to be the lowest energy path for all the energy refinements, and the T_1 diagnostic is low enough to expect an accurate result after CCSD(T) refinement. However the calculated rate constants for the TS-RDFT are in the range $(1.19\text{-}4.01)\times10^{-21}\frac{\mathrm{cm}^3}{\mathrm{s}}$) which is three orders of magnitude lower than the experimental value. The poor agreement with experiment might suggest that another mechanism with a lower energy barrier exists, but we were unable to find other transition states using the (R/U)DFT optimization methods. Interestingly, CCSD(T) predicts the lowest energy barrier of all the refinement methods, but when comparing to the experimental result, there is no reason to believe it under-predicts the energy barrier for the reaction. If the RDFT is assumed to yield accurate geometries for the TS, it might indicate that higher order excitation is important for the CCSD(T) wavefunction, and expanding the excitation operator to include triples and quadruples might improve the quality of the calculated energy barriers. However, such investigation lies outside the scope of this work.

2-methylbutene

2-methylbutene is an asymmetric alkene where addition of singlet oxygen may occur on the doubly substituted side of the alkene (*cis*-TS) or on the mono-substituted side (*trans*-TS) as illustrated in Figure 21.

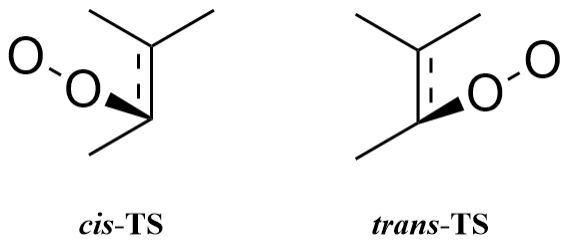

Figure 21: Illustration of the *cis*- and *trans*-addition of singlet oxygen to 2-methylbutene.

cis-Addition

The *cis*-TS is believed to be the most favourable pathway for the 2-methylbutene reaction.[17,44] The stereoselectivity of the reaction has been studied by Stratakis et al. by substituting hydrogen with deuterium as is shown in Figure 22.

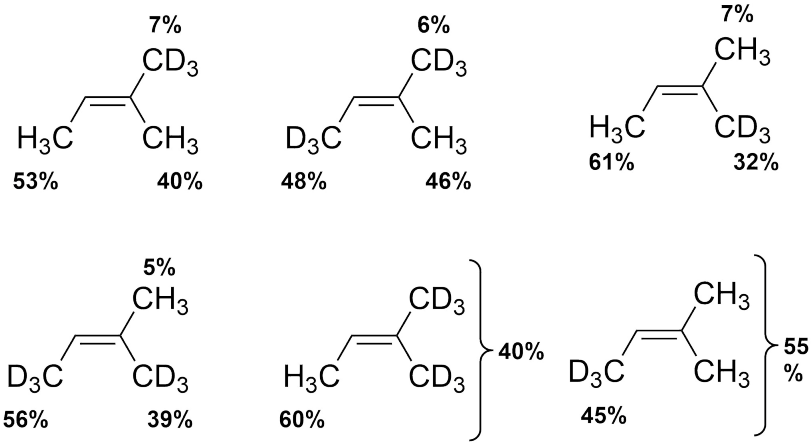

Figure 22: Stereo selectivity of 2-methylbutene.[17]

The *cis*-effect is evident from their results, and the clear change of stereoselectivity of the different deuterated 2-methylbutene derivates is evidence for the formation of a perepoxide

intermediate in this mechanism.[17] The proposed mechanism for the two major reaction paths is shown in Figure 23.

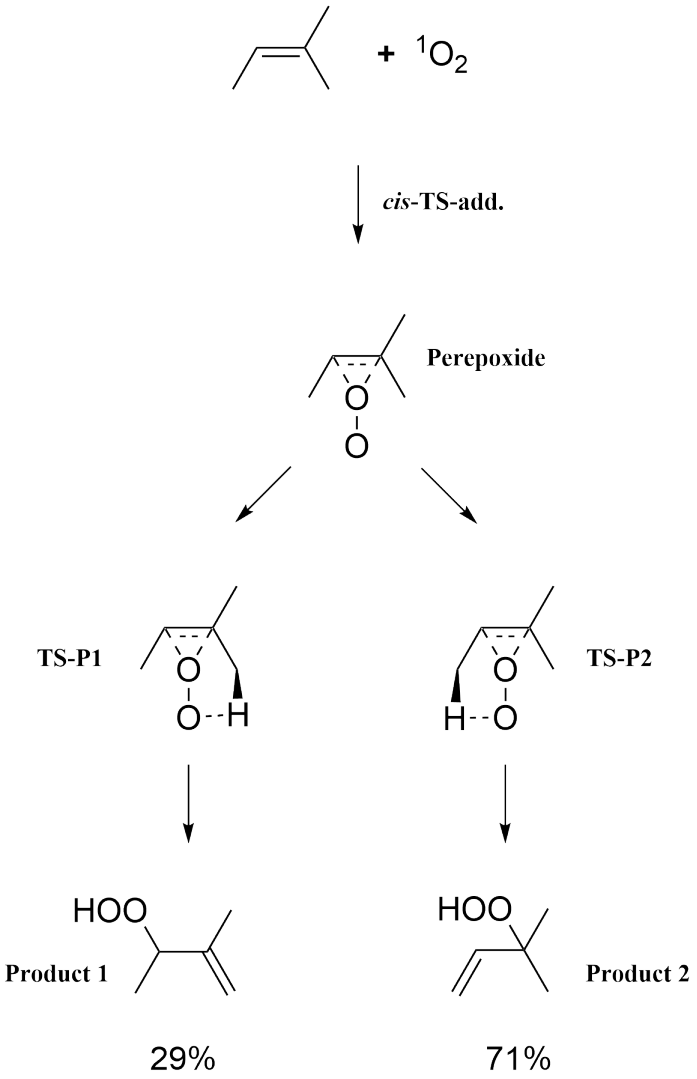

Figure 23: Illustration of the *cis*- and *trans*-addition of singlet oxygen to 2-methylbutene, together with the gas-phase yield of the two products.[43]

Subsequent theoretical studies by Singleton et al. found the mechanism to proceed through two transition states but without any stable intermediate between the two TS's.[44] The rate determining step was found to be the first TS (*cis*-TS-add), where oxygen adds to the alkene, but without hydrogen abstraction. The initial TS has a "perepoxide-like" structure, however the perepoxide is not a stable intermediate since TS-P1 and TS-P2, leading to the two major products are lower in energy compared to the perepoxide. In the following

section we compare our result with the experimental evidence and the theoretical results of singleton et al.[44]

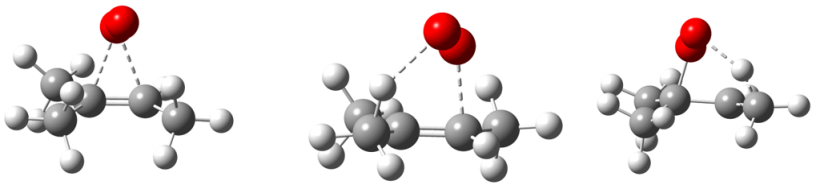

Figure 24: TS structure of *cis*-TS-RDFT (left), TS-RDFT-Hshift1 (middle) and TS-RDFT-Hshift2 (right), calculated at the (R)M06-2X/AVTZ level of theory.

Our M06-2X/AVTZ TS structures for the *cis*-addition are shown in Figure 24. The B3LYP-D3/AVTZ method failed to find TS-P1, and therefore the M06-2X/AVTZ geometries are shown instead. The refined energies of the optimized geometries for the *cis*-addition are shown in Table 5. The reaction mechanism is a stepwise addition of singlet oxygen, where no stable intermediate is formed in the reaction. The first TS (*cis*-TS-add) is an addition of singlet oxygen to the double bond in the alkene. *cis*-TS-add has a "perepoxide-like" structure but the energy of the perepoxide intermediate is higher compared to the energy of TS-P1 and TS-P2. Note that TS-P1 and TS-P2 leads to two different hydroperoxide products via hydrogen abstraction. The energy of TS-P2 to lower than TS-P1 indicating that product 2 is favored over product 1 in perfect agreement with the product yield observed in the studies of Stratakis et al. and Ashford et al.[17,43] The energy barriers for *cis*-TS-add are shown in Table 6 alongside the spin contamination, T_1 diagnostics and rate constants. Interestingly, the UDFT solution collapse to the RDFT solution for both B3LYP-D3/AVTZ and ωB97XD/AVTZ, and with only a slight spin contamination observed with the M06-2X/AVTZ method. The biradical pathway, predicted by UDFT for the previous systems was not found for the *cis*-addition. The T_1 diagnostics are under 0.03 for all found TS.

Table 5: Energies for the optimized stationary points of the *cis*-addition, the electronic energy is refined with method 2.

relative energies including ZPVE	*cis*-TS	Perepoxide	TS-P1	TS-P2
RM062X	3.66	1.49	0.01	-0.53
RωB97XD	5.08	1.31	-0.38	-1.09
RB3LYP-D3	3.51	-	-	-
UM062X	3.47	1.49	0.01	-0.53
UωB97XD	5.08	1.31	-0.38	-1.09
UB3LYP-D3	3.49	-	-	-

We will now focus on the two IRCs obtained using B3LYP-D3/AVTZ that lead to formation of product 2.

Figure 25 shows S_0, S_1, S_2 and T_0 refined by CASPT2/AVTZ and MRCI+Q/AVTZ for the IRC obtained for *cis*-TS-add and TS-P2. Unfortunately, it was not possible to connect the two IRCs directly through a common intermediate, which is clearly seen in the discontinuity observed between the two reaction coordinates. This problem likely originates from the flat typography of the potential energy surface in this region. It was not possible to obtain an IRC going from (*cis*-TS-add) towards the reactant region. A scan was calculated by constraining the C-O bond length while optimizing all other degrees of freedom, however this calculation failed to converge. We argue that the reasonable quality of the RDFT optimized transition states for the other systems, justifies its use for this reaction.

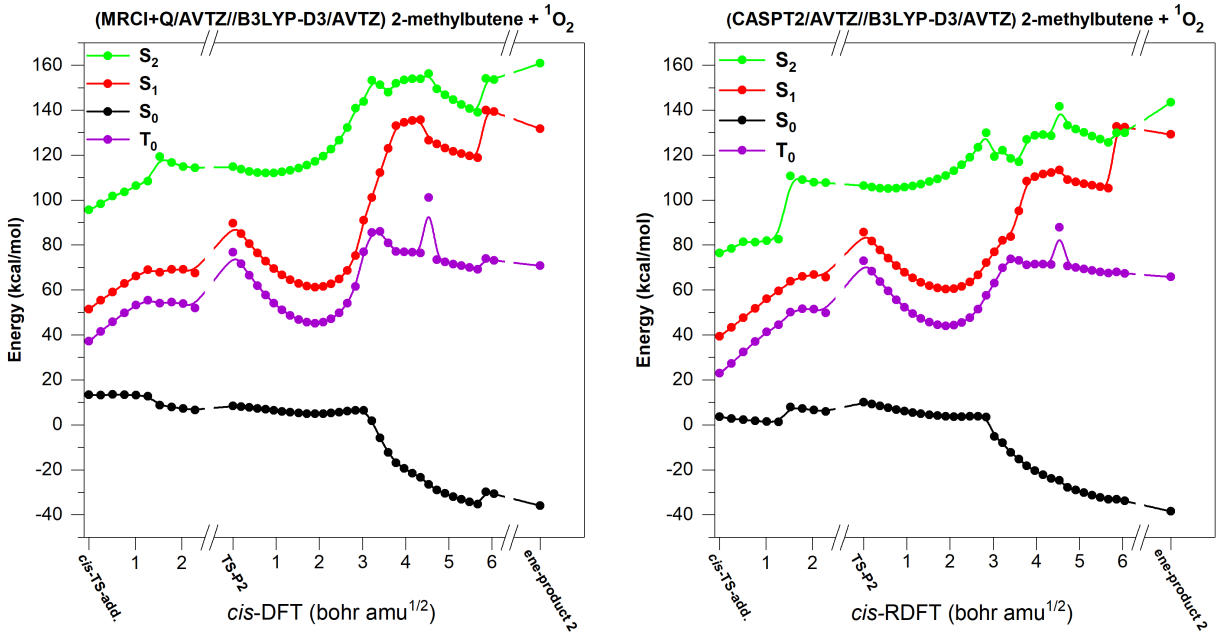

Figure 25: S_0, S_1, S_2 and T_0 electronic energy surfaces calculated by method 1 along the reaction coordinate of *cis*-TS-add and TS-P2.

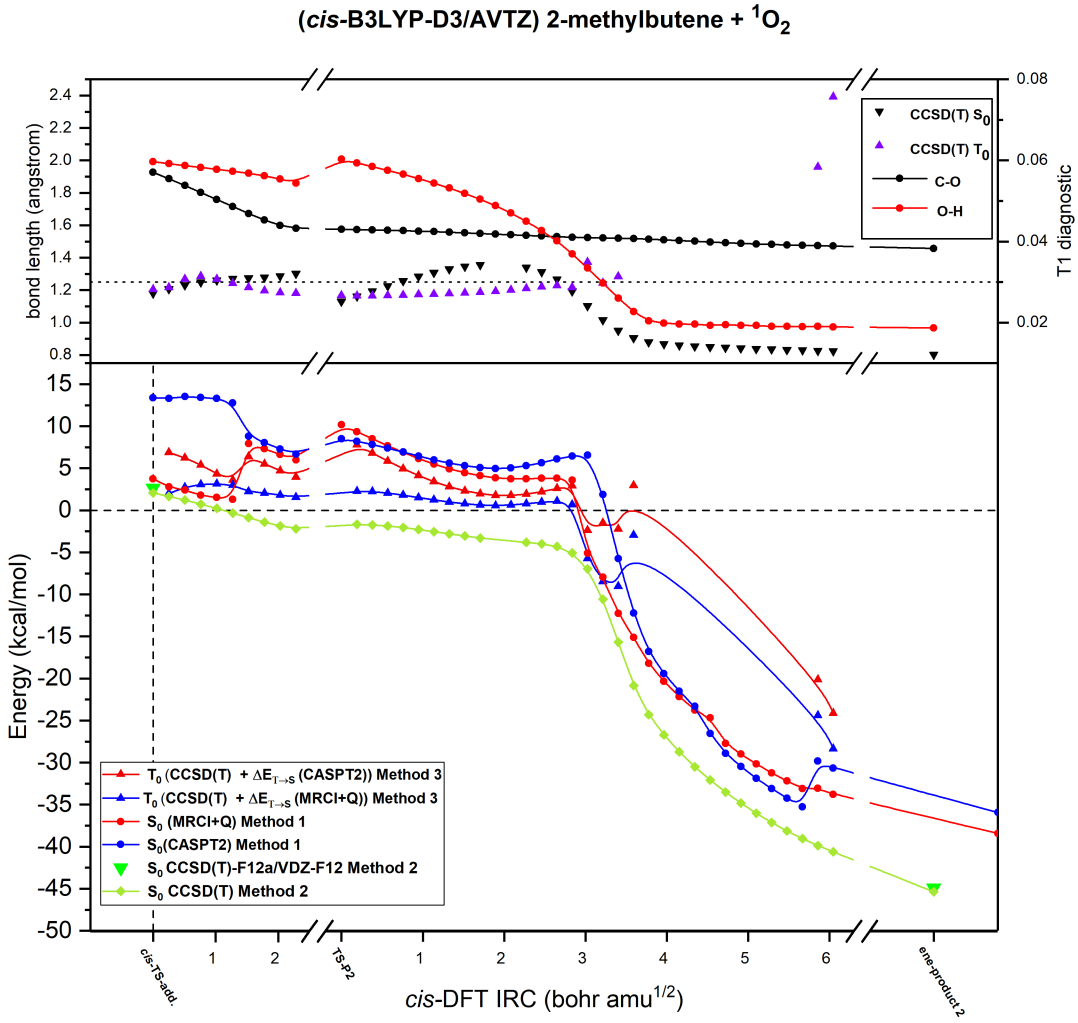

Figure 26: Lower panel Energy refinement of S_0 by method 1, 2 and 3, along the reaction coordinate for *cis*-TS-add and TS-P2. Upper panel T_1 diagnostic of S_0 and T_0, and C-O and O-H bond length along the same reaction coordinate.

The energy refinement of the IRC show that S_0 is the lowest electronic state and that the S_0 and T_0 surfaces intersect before *cis*-TS reached. The energy differences between S_0 and S_1 at the *cis*-TS are 35.73 kcal/mol (CASPT2/AVTZ) and 38.14 kcal/mol (MRCI+Q/AVTZ). This is a larger energy separation between S_0 and S_1 than for the transition states of propene, 2methylporpene and *trans*-butene, indicating a lower multi-reference character for the *cis*-TS compared to the previously identified transition states. Figure 26 shows the T_1 diagnostic

along the reaction coordinate obtained using B3LYP-D3/AVTZ. The T_1 of S_0 increases after *cis*-TS-add, to values slightly over 0.03. The T_1 diagnostic for TS-P2 is less than 0.03 but increases above 0.03 as the reaction proceeds. The S_0 surface is very flat until the point of hydrogen abstraction. As seen in Figure 26 the *cis*-TS IRC describes the formation of the C-O bond while TS-P2 describes the formation of the O-H bond. The refined energy of (*cis*-TS-add) is 3.75 CASPT2/AVTZ (method 1), 13.38 MRCI+Q/AVTZ (method 1), 2.07 CCSD(T)/AVTZ (method 2), 6.87 CCSD(T)/AVTZ+CAPT2/AVTZ (method 3) and 3.17 kcal/mol CCSD(T)/AVTZ+(MRCI+Q/AVTZ) (method 3). The reaction coordinate at the MRCI+Q and CASPT2 levels show discontinuities which affect the reliability of these results. The reaction coordinate at CCSD(T)/AVTZ (method 2), on the other hand, shows a smooth surface alignment with the results from the DFT optimization.

We now consider the differences between the DFT methods. The calculated energy barrier for *cis*-TS-add optimized with M06-2X/AVTZ, B3LYP-D3/AVTZ and ωB97XD/AVTZ after CCSD(T)-F12a/VDZ-f12 refinement is (3.49-5.13) kcal/mol (Table 6). The calculated rate constant for the reaction is in the range of (9.58-326)$\times 10^{-19}$ $\frac{\text{cm}^3}{\text{s}}$ thus spanning 2 orders of magnitude. The best agreement is obtained using the CCSD(T)/AVTZ//B3LYP-D3/AVTZ method which is within a factor 2 of the experimentally determined rate constant. As before we see that the calculated rate constants are too low, which might indicate that a higher level of theory is needed to obtain accurate energy barriers.

Table 6: Calculated spin contamination($\langle S^2 \rangle$), T_1 diagnostics and energy barriers calculated at the CCSD(T)-F12a/VDZ-F12//DFT/AVTZ level of theory using method 2 for energy refinement (E_0) and rate constants k.

2-methylbutene+ $^1O_2$ *cis*	$\langle S^2 \rangle$	T_1	E_0 (kcal/mol)	k ($\frac{cm^3}{s}$)
RM06-2X		0.022	4.69	1.83×10^{-18}
RM06-2X*		0.022	4.66	2.02×10^{-18}
RωB97XD		0.021	5.08	9.57×10^{-19}
RωB97XD*		0.021	5.13	8.72×10^{-19}
RB3LYP-D3		0.027	3.51	1.24×10^{-17}
RB3LYP-D3†		0.027	2.94	3.26×10^{-17}
UM06-2X	0.022	0.023	4.39	3.10×10^{-18}
UωB97XD	0.000	0.021	5.08	9.58×10^{-19}
UB3LYP-D3	0.000	0.027	3.49	1.28×10^{-17}
Exp.[45]				5.48×10^{-17}

$*$: The geometry optimization was performed using the superfine grid.
†: Energy refined with CCSD(T)/AVTZ.

trans-Addition

We now consider the *trans*-addition of singlet oxygen to 2-methylbutene.

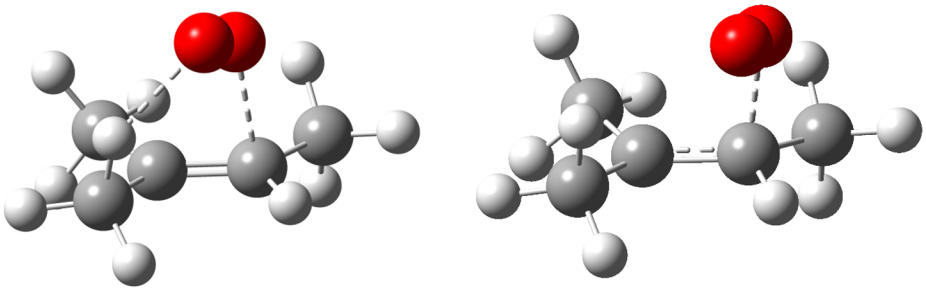

Figure 27: TS structure for *trans*-TS-RDFT (left) and *trans*-TS-UDFT (right), calculated at (R/U)M06-2X/AVTZ level of theory.

The optimized transition states are shown in Figure 27. The *trans*-TS-RDFT follows a concerted reaction path leading directly to the hydroperoxide product, while the *trans*-TS-UDFT calculation predicts a step wise addition forming a biradical/zwitterionic intermediate followed by hydrogen abstraction, leading to the hydroperoxide product.

trans-TS-RDFT

Figure 28 shows the refined energies of S_0, S_1, S_2 and T_0 for the *trans*-TS-RDFT IRC.

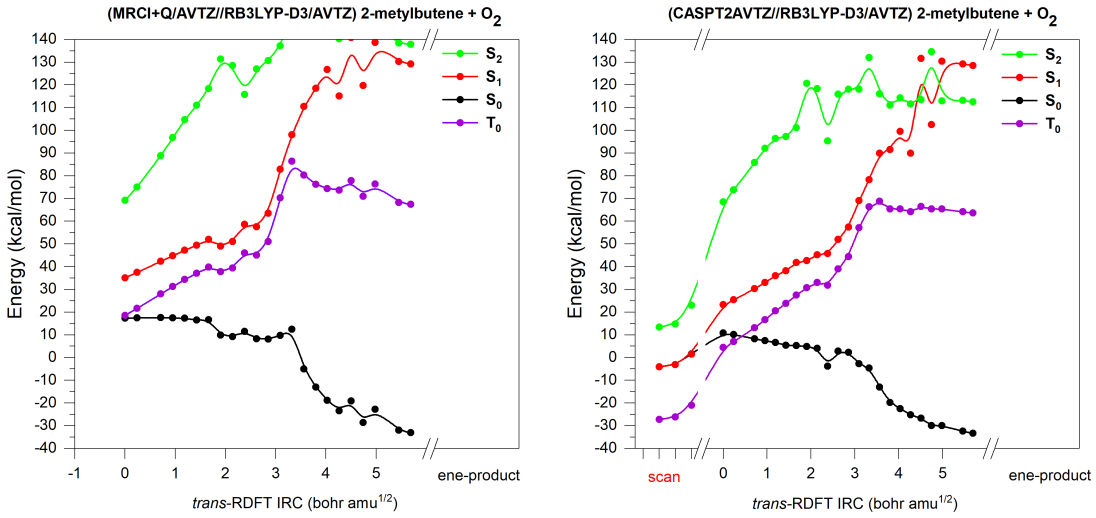

Figure 28: S_0, S_1, S_2 and T_0 electronic energy surfaces calculated by method 1 along the reaction coordinate of *trans*-RDFT.

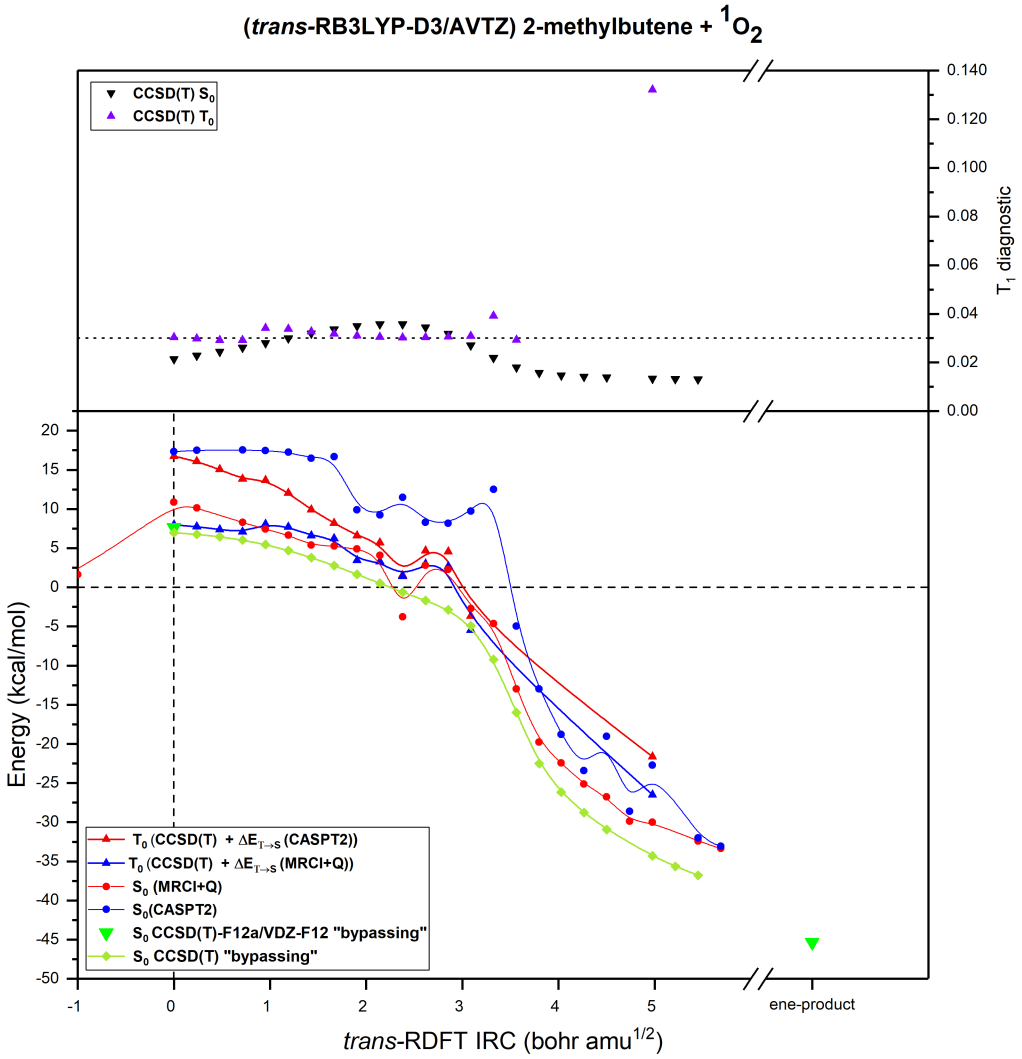

Figure 29: Lower panel Energy refinement of S_0 by method 1, 2 and 3, along the reaction coordinate for *trans*-TS-RDFT. Upper panel T_1 diagnostic of S_0 and T_0 along the same reaction coordinate.

The IRC could only be obtained in the product direction. The S_0 and T_0 surfaces intersect near the TS, and the energy difference between S_0 and S_1 is 12.49 kcal/mol (CASPT2/AVTZ) and 17.78 kcal/mol (MRCI+Q/AVTZ). The bumpy appearance of the energy surface might indicate that the size of the active space is insufficient to describe the entire reaction surface. This may be due to the limited inclusion of correlation energy in the CASPT2 and MRCI+Q methods. The potential energy surface close to the TS seems to be well behaved and is used

to refine the energy of the TS. Figure 29 shows the refined energy of S_0. The refined energy of the TS is 10.85 CASPT2/AVTZ (method 1), 17.32 MRCI+Q/AVTZ (method 1), 6.96 CCSD(T)/AVTZ (method 2), 16.75 CCSD(T)/AVTZ+CAPT2/AVTZ (method 3) and 7.98 kcal/mol CCSD(T)/AVTZ+(MRCI+Q/AVTZ) (method 3). The refined energies are seen to vary up to 10 kcal/mol across the energy refinement methods.

trans-TS-UDFT

Figure 30 shows the surfaces S_0, S_1, S_2 and T_0 for *trans*-TS-UDFT.

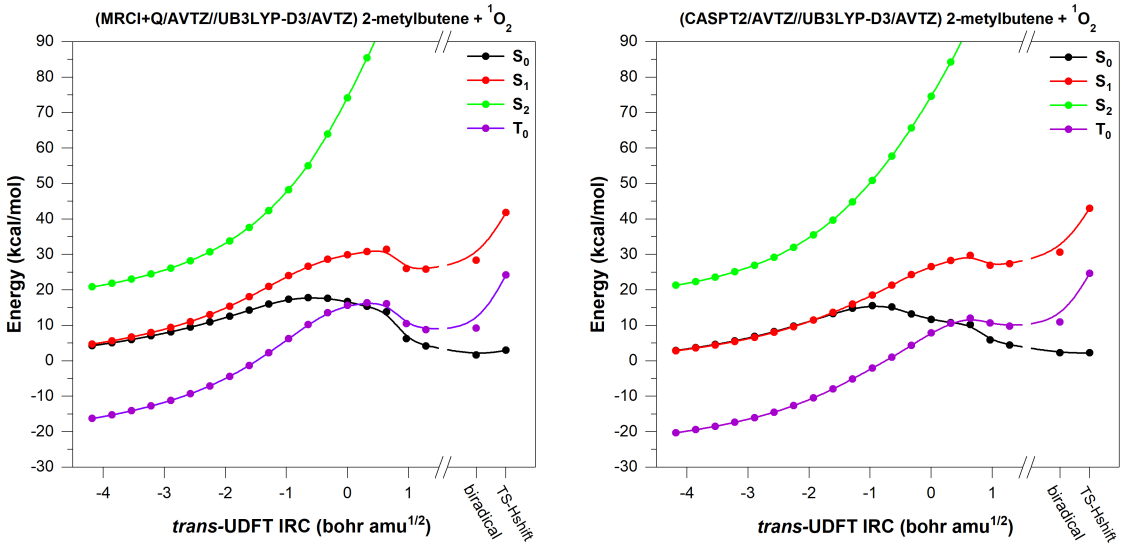

Figure 30: S_0, S_1, S_2 and T_0 electronic energy surfaces calculated by method 1 along the reaction coordinate of *trans*-UDFT.

The qualitative trends for this reaction surface are very similar to the ones obtained for *cis*-propene-UDFT, UDFT-2-methylpropene and UDFT-*trans*-butene: S_0, S_1 and T_0 stay energetically close along the reaction coordinate. The TS energy difference between S_0 and S_1 is 14.90 (CASPT2/AVTZ) and 13.22 kcal/mol (MRCI+Q/AVTZ) while the energy difference between S_0 and T_0 is 3.81 (CASPT2/AVTZ) and 1.09 kcal/mol (MRCI+Q/AVTZ). Figure 31 shows the refined S_0 energies. All the energy refinements predict an earlier TS compared to the optimized UDFT-TS. The maximum for the energy barrier is 15.49 CASPT2/AVTZ (method 1), 11.29 MRCI+Q/AVTZ (method 1), 11.42 CCSD(T)/AVTZ

(method 2), 18.17 CCSD(T)/AVTZ + CASPT2/AVTZ (method 3) and 11.87 kcal/mol CCSD(T)/AVTZ+(MRCI+Q/AVTZ) (method 3).

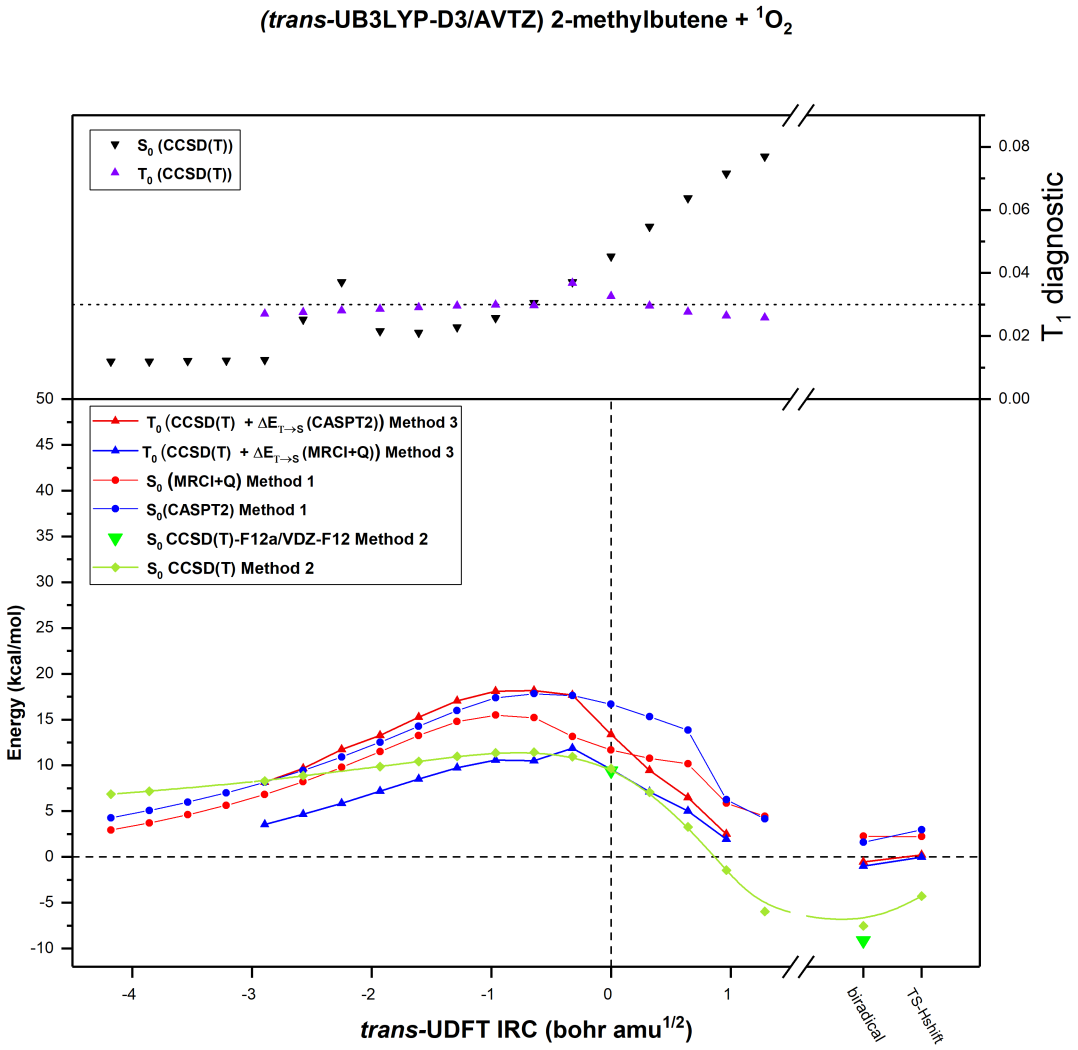

Figure 31: Lower panel Energy refinement of S_0 by method 1, 2 and 3, along the reaction coordinate for *trans*-TS-UDFT. Upper panel T_1 diagnostic of S_0 and T_0 along the same reaction coordinate.

It is seen that the values of the T_1 diagnostics for the S_0 surface tend to increase along the reaction coordinate reaching values much larger than 0.03 towards the product region. The T_1 diagnostic values of T_0 on the other hand stay low along the reaction path and should give reliable results.

Table 7: Calculated spin contamination($\langle S^2 \rangle$), T_1 diagnostic values and energy barriers calculated using CCSD(T)-F12a/VDZ-F12//DFT/AVTZ and method 2 for energy refinement (E_0) and rate constants k.

2-methylbutene + $^1O_2$ *trans*	$\langle S^2 \rangle$	T_1	E_0 (kcal/mol)	k ($\frac{cm^3}{s}$)
RM06-2X		0.022	7.91	2.54×10^{-20}
RM06-2X*		0.022	7.89	2.52×10^{-20}
RωB97XD		0.022	8.30	1.45×10^{-20}
RωB97XD*		0.022	8.24	3.22×10^{-20}
RB3LYP-D3		0.022	8.27	1.37×10^{-20}
UM06-2X	0.963	0.048	12.40	7.18×10^{-23}
UωB97XD	0.982	0.057	12.72	3.78×10^{-23}
UB3LYP-D3	0.866	0.051	9.56	3.92×10^{-21}
Exp.[45]				5.48×10^{-17}

$*$: The geometry optimization was performed using the superfine grid.

The energeries of the optimized *trans*-TS, calculated using CCSD(T)-F12a/VDZ-F12 are presented in Table 6. The calculated rate constants are 2-3 orders of magnitude lower than those calculated for the *cis*-addition, in qualitative agreement with the experimental trend, where products originating from the *cis*-addition are the major products.

2,3-dimethylbutene

The reaction of 2,3-dimethylbutene with singlet oxygen is a well studied system. Different mechanisms have been proposed. In particular the kinetic isotope effect indicated the mechanism is occurring via the perepoxide intermediate.[18] Theoretical results indicate that the perepoxide intermediate is not a true intermediate since its energy is larger than the transition state which via hydrogen abstraction lead to the ene-product. The reaction proceeds through a two step mechanism with no stable intermediate similar to 2-methylbutene.[44] However later theoretical results showed that solvent effect stabilize the perepoxide intermediate which transform the reaction to a stepwise addition with formation of a perepoxide intermediate solvent.[46]

Multiple experimental determinations of the gas-phase rate constant for the 2,3-dimethylbutene reaction with singlet oxygen have been made.[45,47–49] The relatively large variation observed between the experiments was explained from atomic oxygen which is only partly removed from the singlet oxygen source. Therefore NO_2 was added to capture the remaining atomic oxygen, and better agreement was observed across the different experiments.[45]

The optimized M06-2X structures for the 2,3-dimethylbutene reaction path are shown in Figure 32. The reaction profile is very similar to that for *cis*-addition to 2-methylbutene. The reaction is found to proceed through two transition states, TS-add describing the addition of singlet oxygen to the double bond, followed by a second transition state (Hshift-TS) describing the hydrogen abstraction which leads to the formation of the hydrogenperoxide product. It was only possible to locate the TS-add using the (R/U)M06-2X/AVTZ and UB3LYP-D3/AVTZ methods. The difficulties in obtaining TS-add might be caused by the low barrier and the unusual shape of the reaction potential. The structures all show low spin-contamination and T_1 diagnostic values, validating the use of method 2 for this system. We were unable to use methods 1 and 3 for energy refinement for this system, since the computational requirements of CASPT2 and MRCI are too high. We were unable to obtain the perepoxide intermediate and Hshift-TS using the B3LYP-D3/AVTZ method. The energy for the reaction paths is shown in Table 8.

Formation of TS-add is the rate determining step of the reaction. The energy barrier of TS-add is (0.79-2.35) kcal/mol and the calculated rate constant is $(4.86\text{-}71.5)\times10^{-16}\frac{\mathrm{cm}^3}{\mathrm{s}}$ which is within a factor of 6 of the experimentally determined rate constant of $12.6\times10^{-16}\frac{\mathrm{cm}^3}{\mathrm{s}}$. The agreement observed between the calculated and experimentally determined rate constant validates the simple approach of method 2 given the low spin contamination and T_1 diagnostic values for the TS.

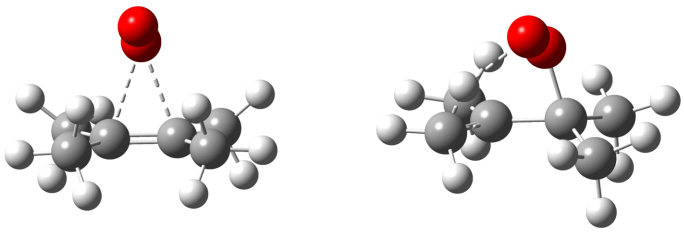

Figure 32: TS structure of TS-add-RDFT (left), TS-RDFT-Hshift (right) calculated at (R)M06-2X/AVTZ level of theory.

Table 8: Energies for the optimized stationary points of the *cis*-addition. The electronic energy is refined with method 2.

relative energies including ZPVE	TS-add	Perepoxide	Hshift-TS
RM062X	2.34	-2.81	-3.86
UM062X	1.61	-2.81	-3.86
UB3LYP-D3	0.79	-	-

Table 9: Calculated spin contamination $\left\langle \hat{S}^2 \right\rangle$, T_1 diagnostic values and and energy barriers calculated with CCSD(T)-F12a/VDZ-F12//DFT/AVTZ using method 2 for energy refinement (E_0) and rate constants k, for the reaction between 2,3-dimethylbutene and singlet oxygen.

2,3-dimethylbutene + $^1O_2$	$\langle S^2 \rangle$	T_1	E_0 (kcal/mol)	k ($\frac{cm^3}{s}$)
RM06-2X		0.019	2.34	6.37×10^{-16}
RM06-2X*		0.019	2.35	4.86×10^{-16}
UM06-2X	0.066	0.021	1.61	2.18×10^{-15}
UB3LYP-D3	0.042	0.023	0.79	7.15×10^{-15}
exp.[45]				1.26×10^{-15}

$*$: The geometry optimization was performed using the superfine grid.

Conclusion

We examined the reaction of a series of five different alkenes with singlet oxygen. The study resulted in two main conclusions.

1) When singlet oxygen adds to alkenes at a position where only one allylic group is available, then two qualitatively different reaction mechanisms are obtained. RDFT predicts that the reaction proceeds through a concerted reaction path where oxygen simultaneously adds to the double bond and abstracts the allylic hydrogen. The UDFT method on the other hand predicts that the reaction proceeds via stepwise addition where oxygen first adds to the double bond forming a biradical/zwiterionic intermediate, followed by hydrogen abstraction to form the ene-product. The tendency of the RDFT method to find a concerted TS and the UDFT method to find non-concerted reaction paths has also been observed for the Diels-Alder reaction between butadiene and ethene.[50] The UDFT wave function for step wise addition is heavily spin contaminated. The spin contamination is mainly from the triplet state and hence a side effect of the spin contamination is to overestimate the biradical character of the optimized geometries. This leads to a later TS compared to the tested energy refinements, which is in agreement with the findings of Saito et al.[41] The poor quality of the UDFT optimized TS leads to an error in the estimated energy barrier of 1-5 kcal/mol, which might lead to qualitatively wrong conclusions regarding the reaction mechanism. We found that the RDFT reaction path was consistently lower in energy than the UDFT path, but the small energy difference means they will both be important. Along the UDFT reaction coordinate the T_0 and S_0 surfaces remain close in energy. If the biradical is a stable intermediate along the UDFT reaction coordinate, quenching back to the triplet reactant might be important, however since the energy barrier going from biradical to ene-product seems to be very low, the reaction might continue to the ene-product without having time to become quenched. The flat nature of the potential energy surface in the TS region could indicate that a finer grid would improve the quality of the optimized geometry, however the optimization performed with the finer grid yielded results similar to the standard grid. The small energy difference between the stepwise addition and the concerted reaction path indicates that these reaction paths will always be in competition and moreover, that they will be differently affected by the solvent. Fudickar et al.[31] showed that the 1,4-cyclo addition went from a

stepwise mechanism to a concerted mechanism when going from gas-phase to an acetonitrile solution using a broken symmetry solution of unrestricted B3LYP and M062X functionals. We argue that similar effects are at work in the ene-mechanism, and so the seeming conflict in the literature simply arises from the close competition between the concerted and step-wise addition pathways. One pathway or the other may become dominant depending on both the solvent and the exact system in question. The poor agreement with the experimental rate constant for *trans*-butene might indicate that a third reaction path with a lower energy exists, however it could not be found with traditional restricted and unrestricted DFT methods.

2) When singlet oxygen adds to an alkene at a position where two allylic groups are *cis* to the double bond, then the reaction occurs through two transition states without a stable intermediate between them. The UDFT and RDFT calculations predict similar reaction paths, and low spin contamination (0.000-0.066) and low T_1 diagnostic (0.019-0.027) are observed in the TS. A good agreement between experimental and theoretical rate constants was observed for these systems. The straightforward bypassing scheme we tested in method 2 is applicable to this type of reaction. Recently, we tested method 2 on a series of 1,4-cycloaddition reactions where we were able to obtain good agreement between experimental and theoretical rate constants. The success of the bypassing scheme of method 2 relies on the multi-reference character being sufficiently low in the TS. In the limit of low spin contamination and T_1 values we believe method 2 is straightforward and can easily be scaled to treat larger molecular systems, as long as the CCSD(T)-F12a/VDZ-F12 single point calculation is feasible.

References

(1) Lane, N. *Oxygen: The molecule that made the world*; Oxford University Press, USA, 2002.

(2) Schmidt, J. A.; Johnson, M. S.; Schinke, R. Carbon dioxide photolysis from 150 to 210 nm: Singlet and triplet channel dynamics, UV-spectrum, and isotope effects. *Proceedings of the National Academy of Sciences* **2013**, *110*, 17691–17696.

(3) Ueno, Y.; Johnson, M. S.; Danielache, S. O.; Eskebjerg, C.; Pandey, A.; Yoshida, N. Geological sulfur isotopes indicate elevated OCS in the Archean atmosphere, solving faint young sun paradox. *Proceedings of the National Academy of Sciences* **2009**, *106*, 14784–14789.

(4) Chapman, S. A theory of upperatmospheric ozone. *Mem. Roy. Meteor.* **1930**, *3*, 103–125.

(5) Harnung, S. E.; Johnson, M. S. *Chemistry and the Environment*; Cambridge University Press, 2012.

(6) Jones, I.; Bayes, K. Energy transfer from electronically excited NO_2. *Chemical Physics Letters* **1971**, *11*, 163 – 166.

(7) Zhang, Y.; Jacob, D. J.; Maasakkers, J. D.; Sulprizio, M. P.; Sheng, J.-X.; Gautam, R.; Worden, J. Monitoring global tropospheric OH concentrations using satellite observations of atmospheric methane. *Atmospheric Chemistry & Physics* **2018**, *18*.

(8) Wayne, R. P. Singlet oxygen in the environmental sciences. *Research on Chemical Intermediates* **1994**, *20*, 395–422.

(9) Manfrin, A.; Nizkorodov, S. A.; Malecha, K. T.; Getzinger, G. J.; McNeill, K.; Borduas-Dedekind, N. Reactive oxygen species production from secondary organic aerosols: The importance of singlet oxygen. *Environmental science & technology* **2019**, *53*, 8553–8562.

(10) Frimer, A. A. The reaction of singlet oxygen with olefins: Tfhe question of mechanism. *Chemical Reviews* **1979**, *79*, 359–387.

(11) Gollnick, K.; Knutzen-Mies, K. Dye-sensitized photooxygenation of 2, 3-dihydrofurans: competing [2+ 2] cycloadditions and ene reactions of singlet oxygen with a rigid cyclic enol ether system. *The Journal of Organic Chemistry* **1991**, *56*, 4017–4027.

(12) Gollnick, K.; Griesbeck, A. Solvent dependence of singlet oxygen/substrate interactions in ene-reactions,(4+ 2)-and (2+ 2)-cycloaddition reactions. *Tetrahedron Letters* **1984**, *25*, 725–728.

(13) Maranzana, A.; Ghigo, G.; Tonachini, G. The $^1\Delta_g$ Dioxygen Ene Reaction with Propene: A Density Functional and Multireference Perturbation Theory Mechanistic Study. *Chemistry–A European Journal* **2003**, *9*, 2616–2626.

(14) Sevin, F.; McKee, M. L. Reactions of 1, 3-cyclohexadiene with singlet oxygen. A theoretical study. *Journal of the American Chemical Society* **2001**, *123*, 4591–4600.

(15) Ghigo, G.; Maranzana, A.; Causà, M.; Tonachini, G. Theoretical mechanistic studies on oxidation reactions of some saturated and unsaturated organic molecules. *Theoretical Chemistry Accounts* **2007**, *117*, 699.

(16) Leach, A. G.; Houk, K.; Foote, C. S. Theoretical prediction of a perepoxide intermediate for the reaction of singlet oxygen with trans-cyclooctene contrasts with the two-step no-intermediate ene reaction for acyclic alkenes. *The Journal of Organic Chemistry* **2008**, *73*, 8511–8519.

(17) Stratakis, M.; Orfanopoulos, M.; Chen, J. S.; Foote, C. S. Reaction profile of the photooxygenation of trisubstituted alkenes. *Tetrahedron Letters* **1996**, *37*, 4105–4108.

(18) Grdina, M. B.; Orfanopoulos, M.; Stephenson, L. Stereochemical dependence of isotope effects in the singlet oxygen-olefin reaction. *Journal of the American Chemical Society* **1979**, *101*, 3111–3112.

(19) Alberti, M. N.; Orfanopoulos, M. The Cyclopropyl Group as a Hypersensitive Probe in the Singlet Oxygen Ene Reaction Mechanism. *Organic Letters* **2008**, *10*, 2465–2468, PMID: 18489176.

(20) Orfanopoulos, M.; Smonou, I.; Foote, C. S. Intermediates in the ene reactions of singlet oxygen and N-phenyl-1, 2, 4-triazoline-3, 5-dione with olefins. *Journal of the American Chemical Society* **1990**, *112*, 3607–3614.

(21) Alberti, M. N.; Orfanopoulos, M. Recent mechanistic insights in the singlet oxygen ene reaction. *Synlett* **2010**, *2010*, 999–1026.

(22) Poon, T. H. W.; Pringle, K.; Foote, C. S. Reaction of Cyclooctenes with Singlet Oxygen. Trapping of a Perepoxide Intermediate. *Journal of the American Chemical Society* **1995**, *117*, 7611–7618.

(23) Frisch, M. J. et al. Gaussian 16, Revision A.03. 2016; Gaussian Inc. Wallingford CT.

(24) Chai, J. D.; H. Gordon, M. Long-range corrected hybrid density functionals with damped atom-atom dispersion corrections. *Physical Chemistry Chemical Physics* **2008**, *10*, 6615–6620.

(25) Zhao, Y.; Truhlar, D. G. The M06 suite of density functionals for main group thermochemistry, thermochemical kinetics, noncovalent interactions, excited states, and transition elements: two new functionals and systematic testing of four M06-class functionals and 12 other functionals. *Theory. Chem. Acc.* **2008**, *120*, 215–241.

(26) Becke, A. D. Density-functional thermochemistry. III. The role of exact exchange. *J. Chem. Phys.* **1993**, *98*, 5648–5652.

(27) Kendall, R. A.; Dunning Jr, T. H.; Harrison, R. J. Electron affinities of the first-row atoms revisited. Systematic basis sets and wave functions. *The Journal of Chemical Physics* **1992**, *96*, 6796–6806.

(28) Yamanaka, S.; Kawakami, T.; Nagao, H.; Yamaguchi, K. Effective exchange integrals for open-shell species by density functional methods. *Chemical physics letters* **1994**, *231*, 25–33.

(29) Saito, T.; Nishihara, S.; Kataoka, Y.; Nakanishi, Y.; Matsui, T.; Kitagawa, Y.; Kawakami, T.; Okumura, M.; Yamaguchi, K. Transition state optimization based on approximate spin-projection (AP) method. *Chemical Physics Letters* **2009**, *483*, 168–171.

(30) Al-Nuâairat, J.; Altarawneh, M.; Gao, X.; Westmoreland, P. R.; Dlugogorski, B. Z. Reaction of Aniline with Singlet Oxygen (O_2 $^1\Delta_g$). *The Journal of Physical Chemistry A* **2017**, *121*, 3199–3206.

(31) Fudickar, W.; Linker, T. Theoretical insights into the effect of solvents on the [4+ 2] cycloaddition of singlet oxygen to substituted anthracenes: A change from a stepwise process to a concerted process. *Journal of Physical Organic Chemistry* **2019**, *32*, e3951.

(32) Al-Nuâairat, J.; Dlugogorski, B. Z.; Gao, X.; Zeinali, N.; Skut, J.; Westmoreland, P. R.; Oluwoye, I.; Altarawneh, M. Reaction of phenol with singlet oxygen. *Physical Chemistry Chemical Physics* **2019**, *21*, 171–183.

(33) Shamasundar, K.; Knizia, G.; Werner, H.-J. A new internally contracted multi-reference configuration interaction method. *The Journal of Chemical Physics* **2011**, *135*, 054101.

(34) Werner, H.-J.; Knowles, P. J. An efficient internally contracted multiconfiguration–reference configuration interaction method. *The Journal of Chemical Physics* **1988**, *89*, 5803–5814.

(35) Schmidt, M. W.; Gordon, M. S. The construction and interpretation of MCSCF wavefunctions. *Annual Review of Physical Chemistry* **1998**, *49*, 233–266.

(36) Pipek, J.; Mezey, P. G. A fast intrinsic localization procedure applicable for abinitio and semiempirical linear combination of atomic orbital wave functions. *The Journal of Chemical Physics* **1989**, *90*, 4916–4926.

(37) Meissner, L. Size-consistency corrections for configuration interaction calculations. *Chemical Physics Letters* **1988**, *146*, 204–210.

(38) Werner, H.-J.; Knowles, P. J.; Knizia, G.; Manby, F. R.; Schütz, M. MOLPRO, version 2012.1, a package of ab initio programs. 2012.

(39) Lee, T. J.; Taylor, P. R. A diagnostic for determining the quality of single-reference electron correlation methods. *International Journal of Quantum Chemistry* **1989**, *36*, 199–207.

(40) Goldsmith, C. F.; Klippenstein, S. J.; Green, W. H. Theoretical rate coefficients for allyl+ HO_2 and allyloxy decomposition. *Proceedings of the Combustion Institute* **2011**, *33*, 273–282.

(41) Saito, T.; Nishihara, S.; Kataoka, Y.; Nakanishi, Y.; Kitagawa, Y.; Kawakami, T.; Yamanaka, S.; Okumura, M.; Yamaguchi, K. Reinvestigation of the reaction of ethylene and singlet oxygen by the approximate spin projection method. Comparison with multireference coupled-cluster calculations. *The Journal of Physical Chemistry A* **2010**, *114*, 7967–7974.

(42) Wallace, L. Band-Head Wavelengths of C_2, CH, CN, CO, NH, NO, O_2, OH, and Their Ions. *The Astrophysical Journal Supplement Series* **1962**, *7*, 165.

(43) Ashford, R.; Ogryzlo, E. Temperature dependence of some reactions of singlet oxygen with olefins in the gas phase. *Journal of the American Chemical Society* **1975**, *97*, 3604–3607.

(44) Singleton, D. A.; Hang, C.; Szymanski, M. J.; Meyer, M. P.; Leach, A. G.; Kuwata, K. T.; Chen, J. S.; Greer, A.; Foote, C. S.; Houk, K. N. Mechanism of Ene Reactions of Singlet Oxygen. A Two-Step No-Intermediate Mechanism. *Journal of the American Chemical Society* **2003**, *125*, 1319–1328.

(45) Huie, R. E.; Herron, J. T. Kinetics of the reactions of singlet molecular oxygen (O_2 $^1\Delta_g$) with organic compounds in the gas phase. *International Journal of Chemical Kinetics* **1973**, *5*, 197–211.

(46) Sheppard, A. N.; Acevedo, O. Multidimensional Exploration of Valley-Ridge Inflection Points on Potential-Energy Surfaces. *Journal of the American Chemical Society* **2009**, *131*, 2530–2540.

(47) Hollinden, G. A.; Timmons, R. B. Electron spin resonance study of the kinetics of the reaction of oxygen ($^1\Delta_g$)) with tetramethylethylene and 2,5-dimethylfuran. *Journal of the American Chemical Society* **1970**, *92*, 4181–4184.

(48) Ackerman, R.; Pitts, J.; Steer, R. Concerning the effect of pressure on the rate of reaction of O_2 ($^1\Delta_g$)) with tetramethylethylene. *Chemical Physics Letters* **1972**, *12*, 526 – 528.

(49) Furukawa, K.; Ogryzlo, E. Quenching of $O_2(^1\Delta_g)$) by organic molecules. *Chemical Physics Letters* **1971**, *12*, 370 – 372.

(50) Isobe, H.; Takano, Y.; Kitagawa, Y.; Kawakami, T.; Yamanaka, S.; Yamaguchi, K.; Houk, K. Extended HartreeFock (EHF) theory of chemical reactions VI: hybrid DFT and post-HartreeFock approaches for concerted and non-concerted transition structures of the DielsAlder reaction. *Molecular Physics* **2002**, *100*, 717–727.

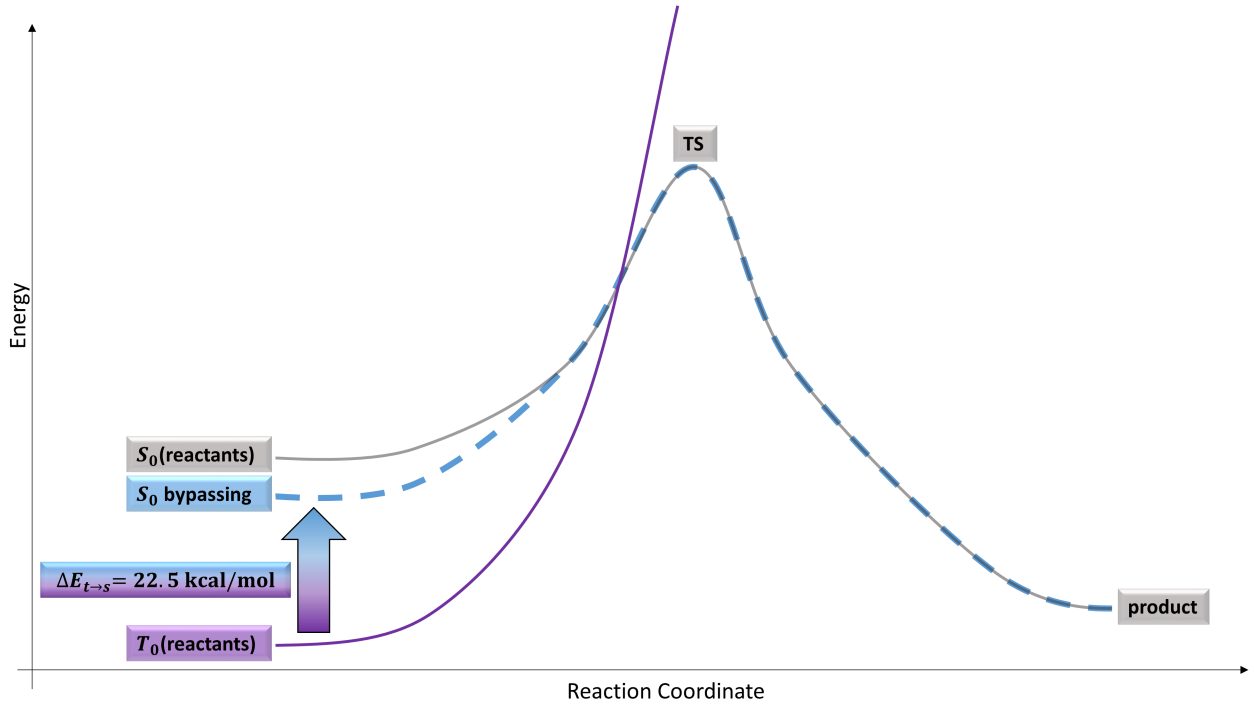

Figure 33: Illustration of the bypassing scheme, T_0 and S_0 are the potential energy surface of the triplet and singlet ground states, calculated with a restricted method. S_0 bypassing is the hypothetical potential energy surface where the error due to the multi-reference character of singlet molecular oxygen is removed. $\Delta E_{t\to s}$ is the experimentally determined singlet/triplet splitting of molecular oxygen.

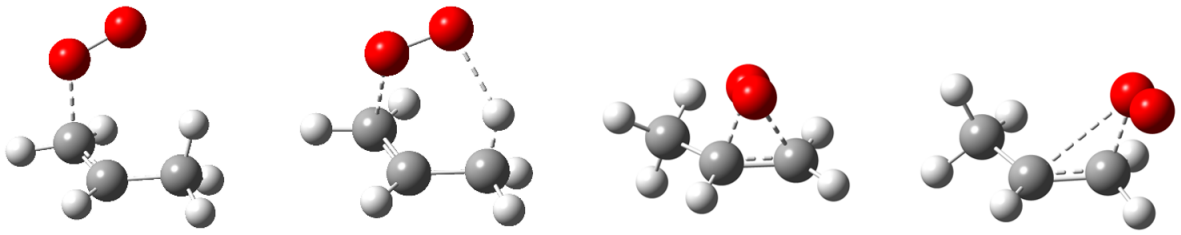

Figure 34: TS structure of *cis*-TS-UDFT (left), *cis*-TS-RDFT (left to the middle), *trans*-TS-RDFT (right to the middle) and *trans*-TS-UDFT (right), calculated at (R/U)B3LYP-D3/AVTZ level of theory.

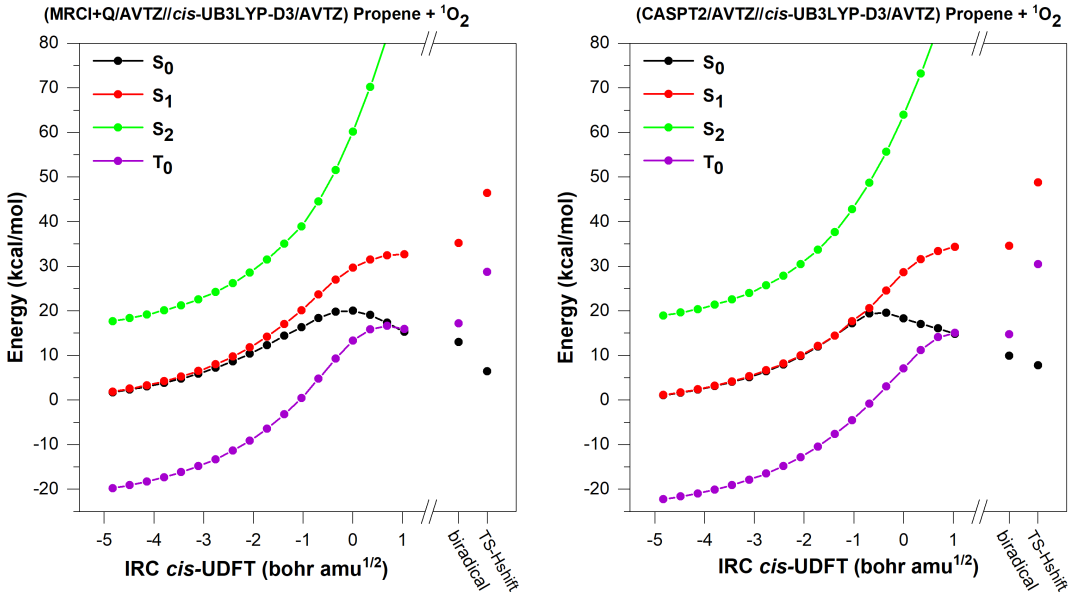

Figure 35: S_0, S_1, S_2 and T_0 electronic energy surfaces calculated by method 1 along the reaction coordinate of *cis*-UDFT.

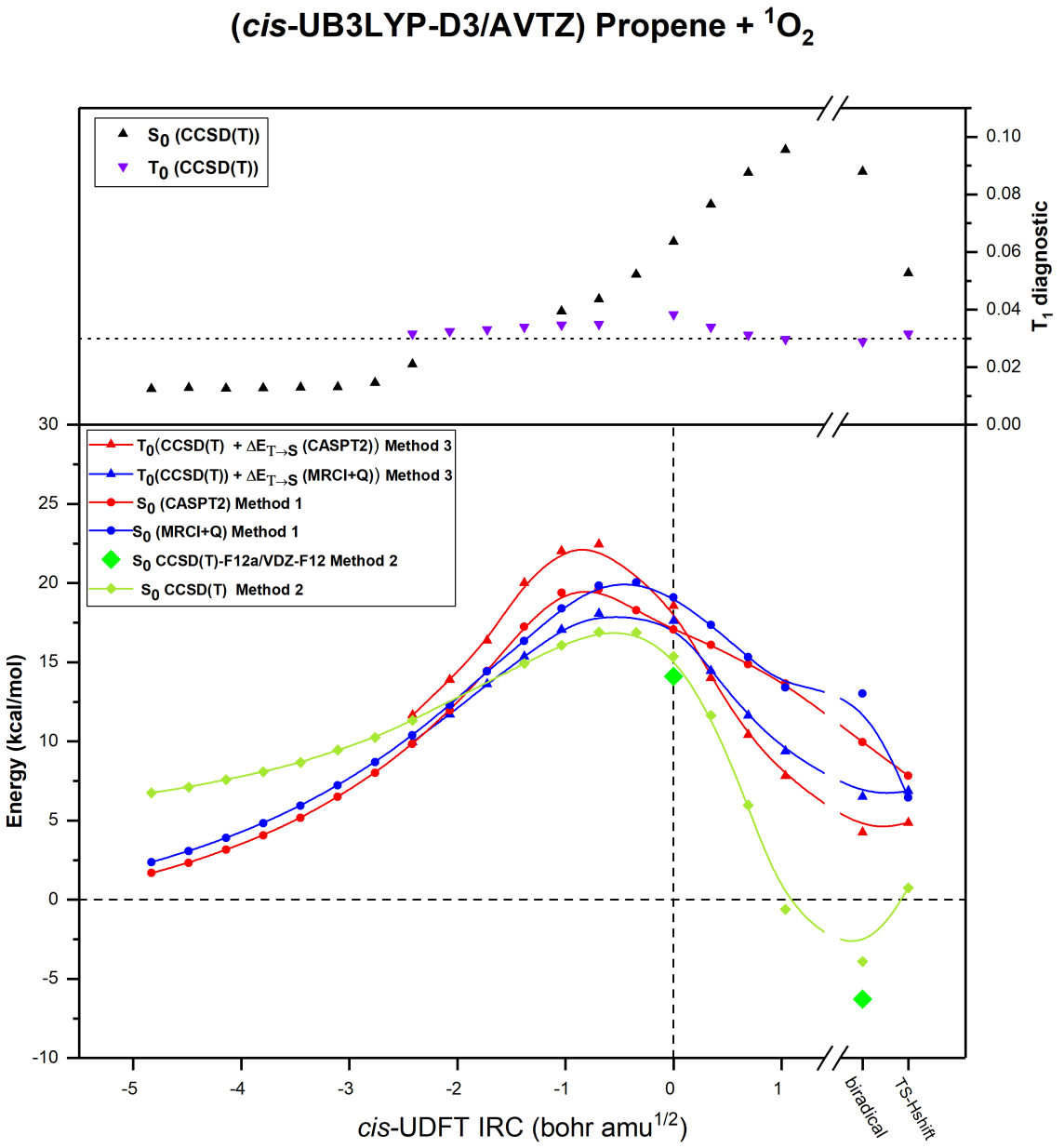

Figure 36: Lower panel Energy refinement of S_0 by method 1, 2 and 3, along the reaction coordinate for *cis*-UDFT propene. Upper panel T_1 diagnostic of S_0 and T_0 along the same reaction coordinate.

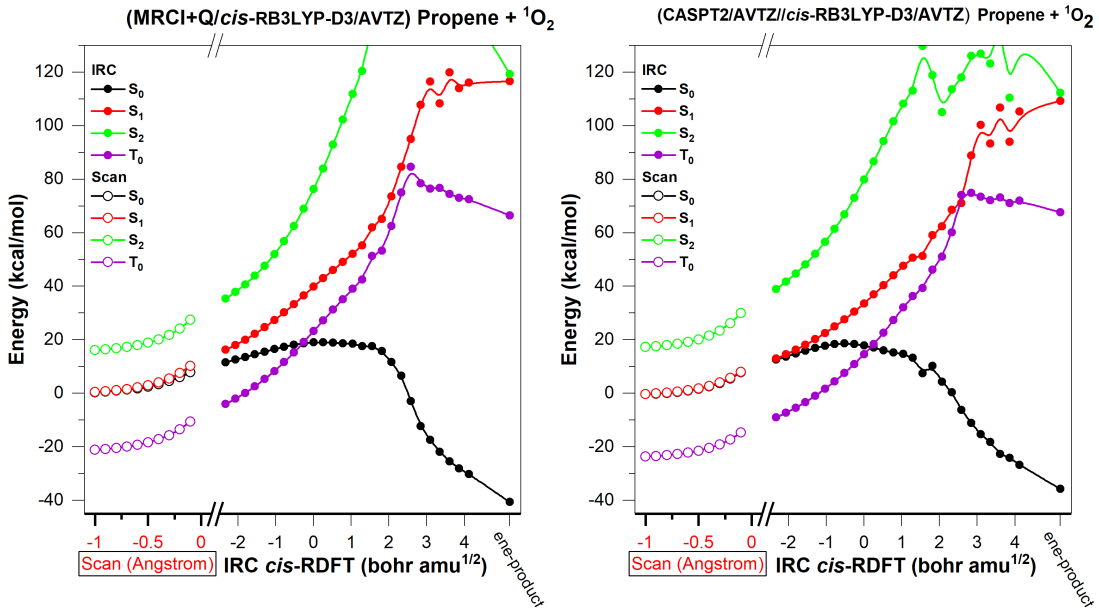

Figure 37: S_0, S_1, S_2 and T_0 electronic energy surfaces calculated by method 1 along the reaction coordinate of *cis*-RDFT.

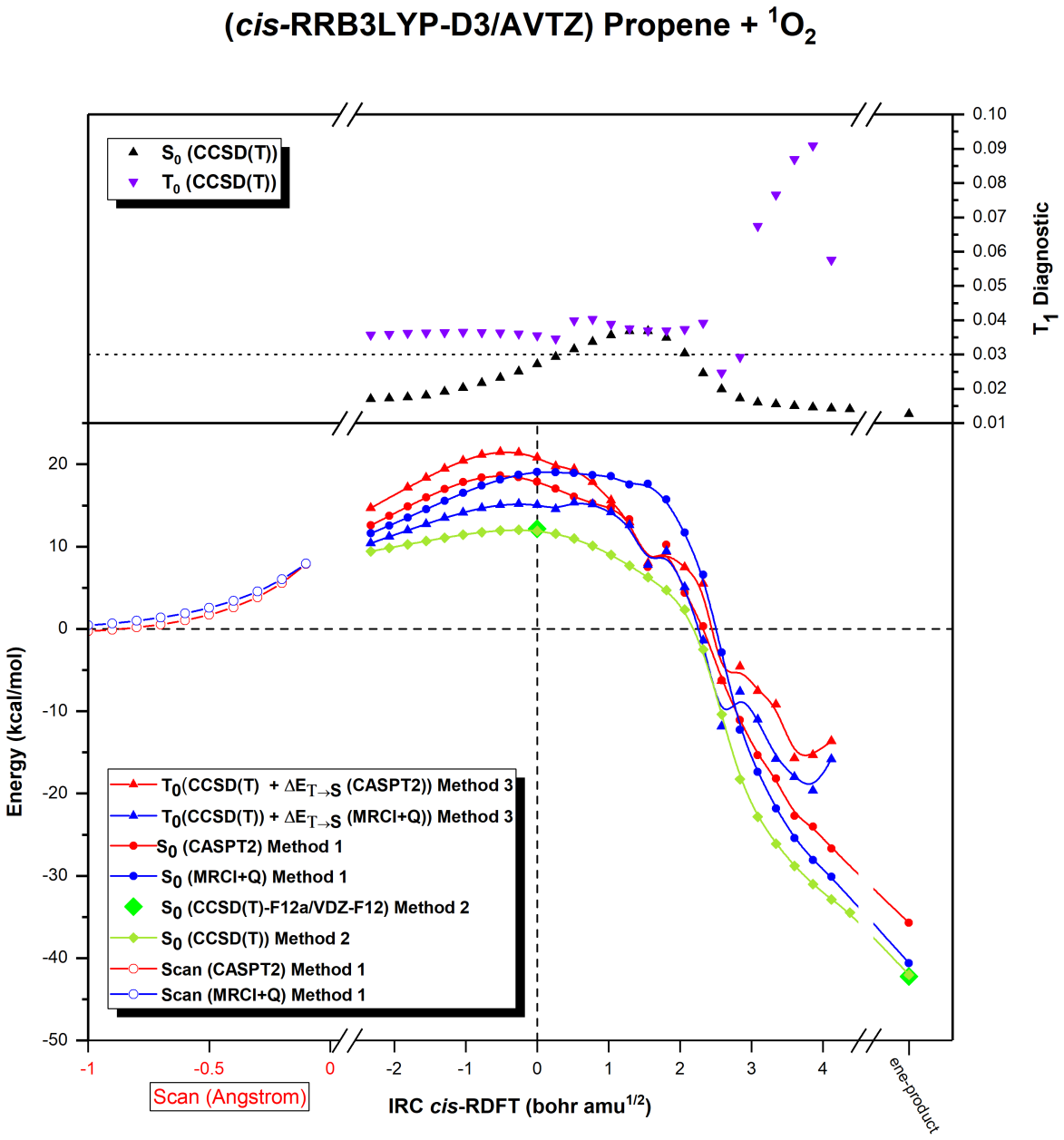

Figure 38: Lower panel Energy refinement of S_0 by method 1, 2 and 3, along the reaction coordinate for *cis*-RDFT propene. Upper panel T_1 diagnostic of S_0 and T_0 along the same reaction coordinate.

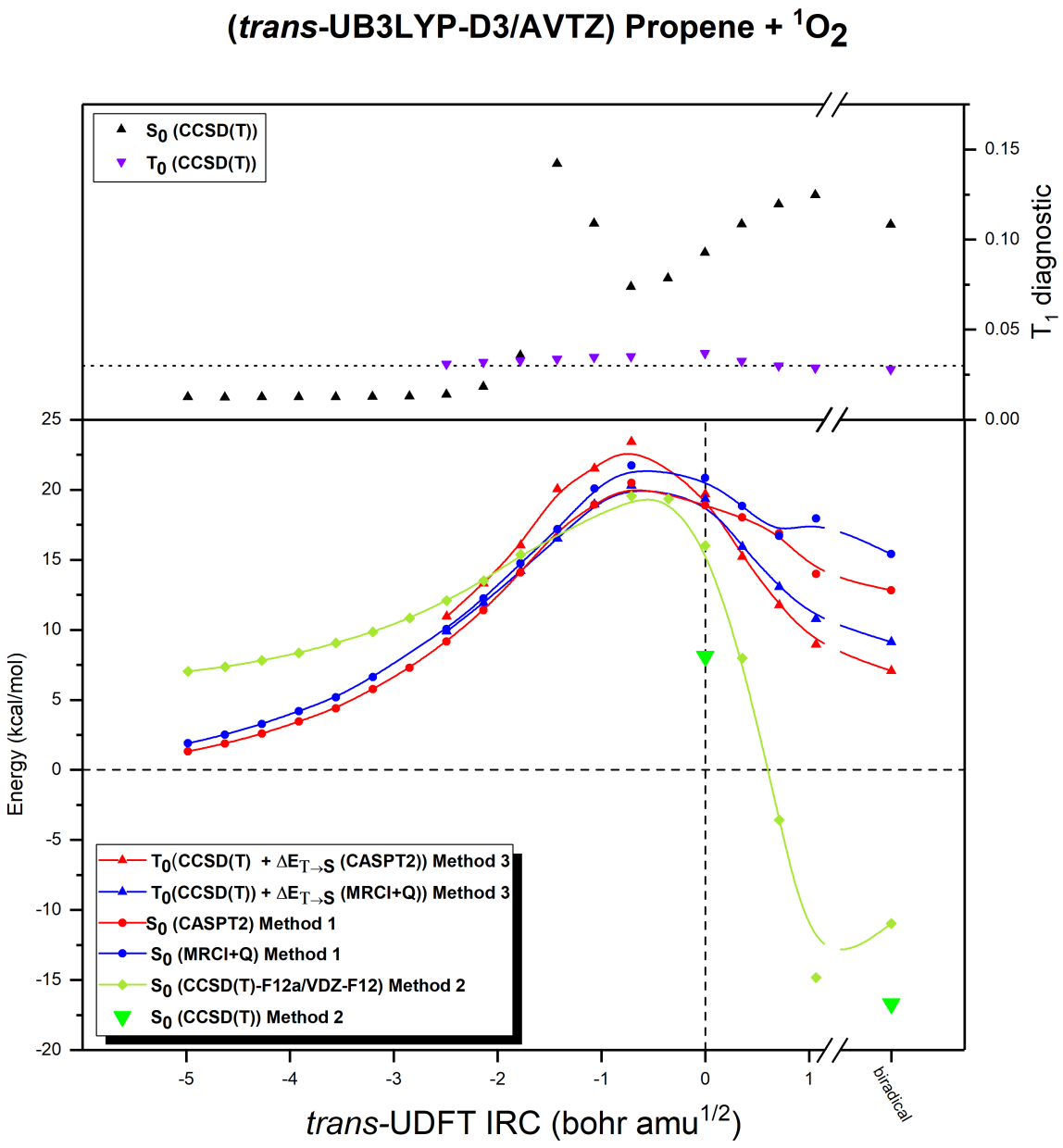

Figure 39: Lower panel Energy refinement of S_0 by method 1, 2 and 3, along the reaction coordinate for *trans*-TS-UDFT propene. Upper panel T_1 diagnostic of S_0 and T_0 along the same reaction coordinate.

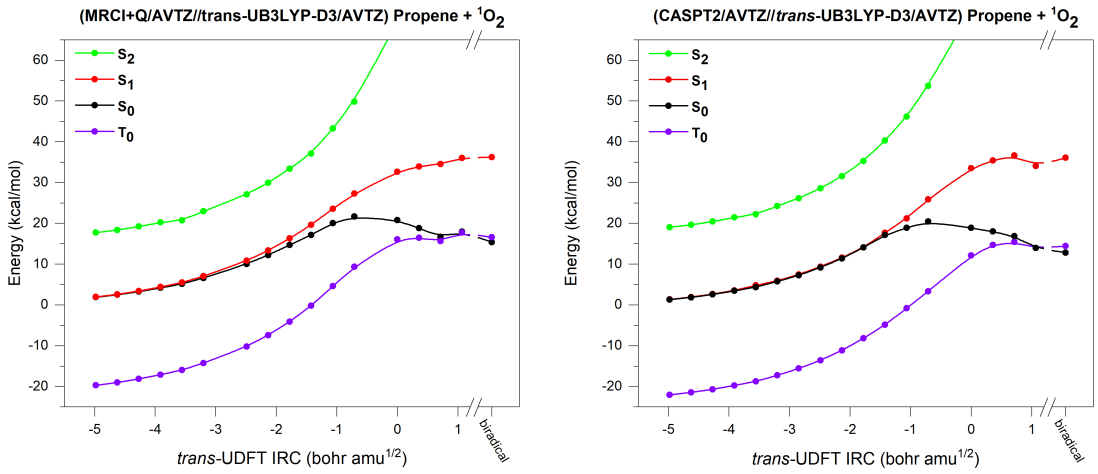

Figure 40: S_0, S_1, S_2 and T_0 electronic energy surfaces calculated by method 1 along the reaction coordinate of *trans*-UDFT.

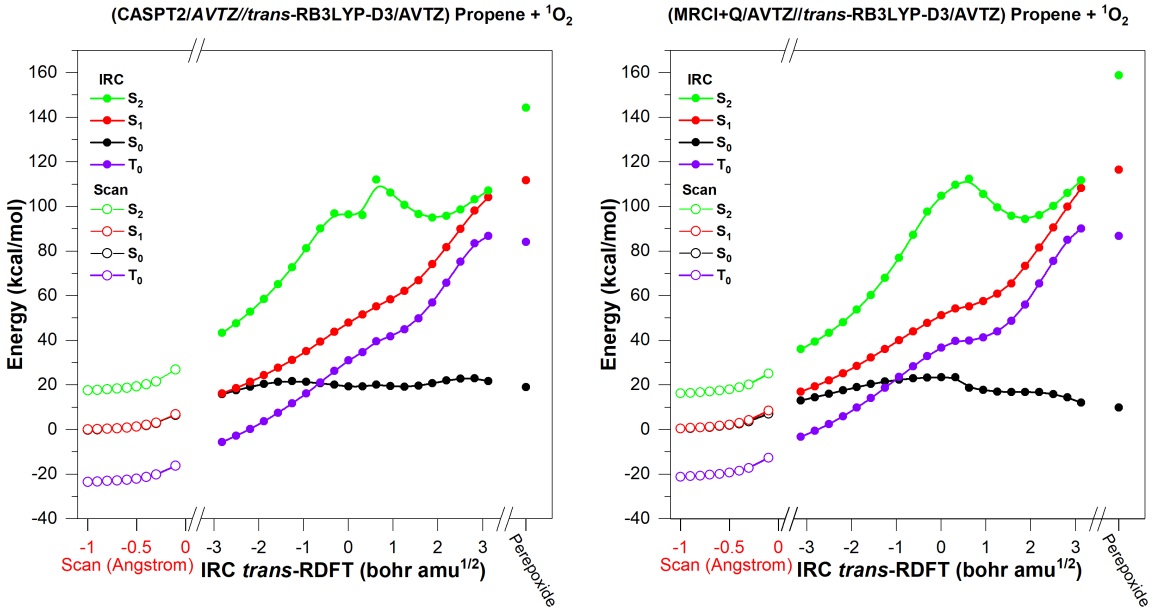

Figure 41: S_0, S_1, S_2 and T_0 electronic energy surfaces calculated by method 1 along the reaction coordinate of *trans*-RDFT.

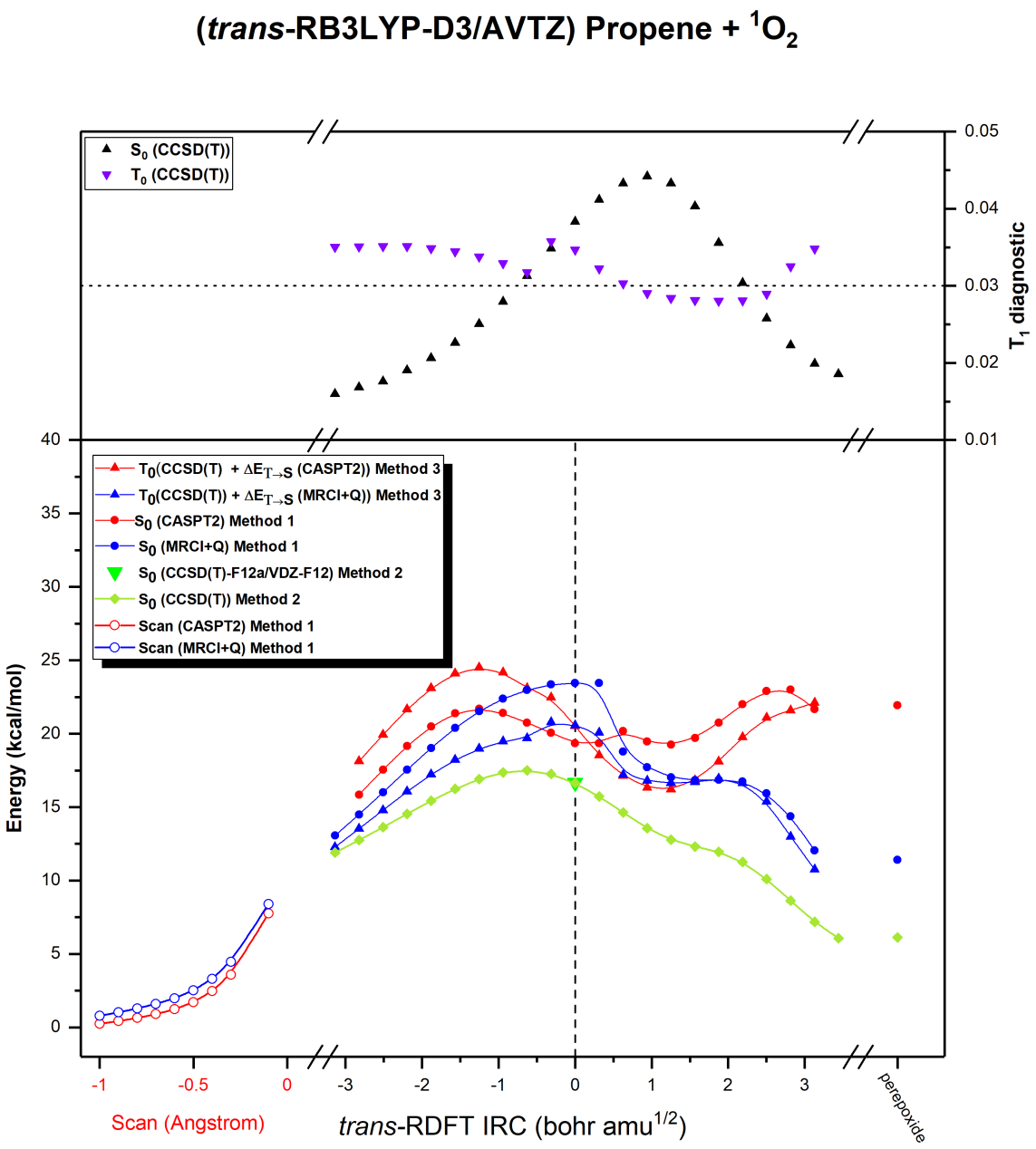

Figure 42: Lower panel Energy refinement of S_0 by method 1, 2 and 3, along the reaction coordinate for *trans*-RDFT propene. Upper panel T_1 diagnostic of S_0 and T_0 along the same reaction coordinate.

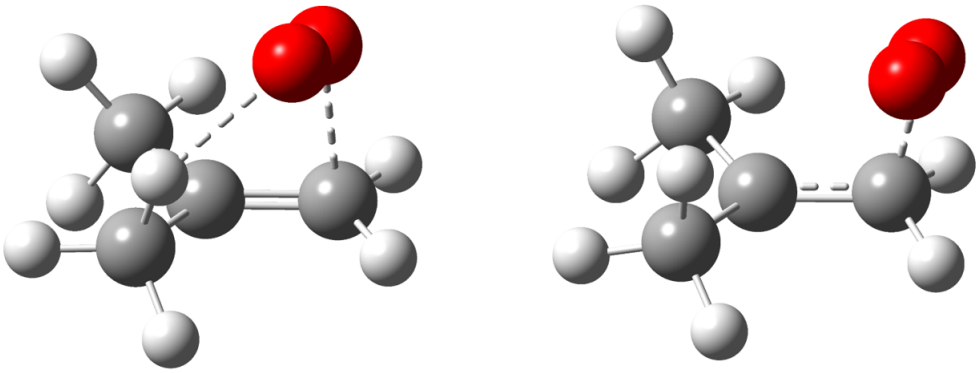

Figure 43: TS structure of TS-RDFT (left) and TS-UDFT (right), calculated at the (R/U)B3LYP-D3/AVTZ level of theory.

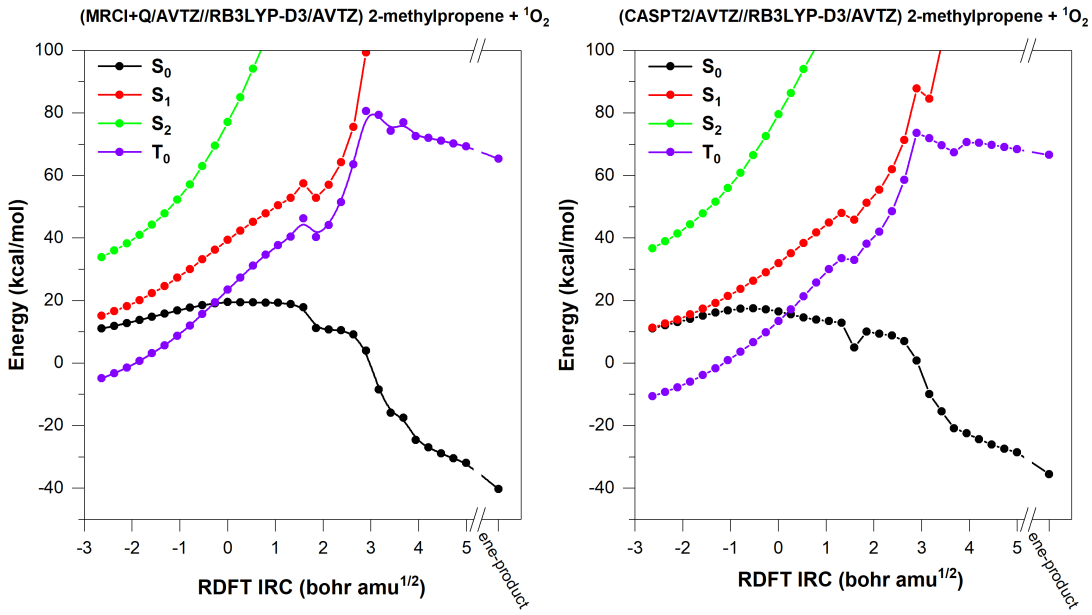

Figure 44: S_0, S_1, S_2 and T_0 electronic energy surfaces calculated by method 1 along the reaction coordinate of TS-RDFT